# Sonic hedgehog enhances calcium oscillations in hippocampal astrocytes

**Chihiro Adachi (足立 ちひろ)[1], Naoto Kakinuma (垣沼 直人)[2], Soohyun Jo (趙 洙賢)[1], Takayuki Ishii (石井 貴之)[1], Yusuke Arai (荒井 祐輔)[1], Satoshi Arai (新井 敏)[3,4], Tetsuya Kitaguchi (北口 哲也)[3,5], Sen Takeda (竹田 扇)[2], and Takafumi Inoue (井上 貴文)[1*]**

[1]Department of Life Science and Medical Bioscience, School of Advanced Science and Engineering, Waseda University, Tokyo, Japan; [2]Department of Anatomy and Cell Biology, Interdisciplinary School of Medicine & Engineering, University of Yamanashi, Yamanashi, Japan; [3]Cell Signaling Group, Waseda Bioscience Research Institute in Singapore (WABIOS), Singapore; [4]Research Institute for Science and Engineering, Waseda University; [5]Laboratory for Chemistry and Life Science, Institute of Innovative Research, Tokyo Institute of Technology, Japan

Running title: SHH enhances Ca oscillations in astrocytes

[*]To whom correspondence should be addressed: Takafumi Inoue: Laboratory of Neurophysiology, Department of Life Science and Medical Bioscience, Faculty of Science and Engineering, Waseda University, 2-2 Wakamatsu-cho, Shinjuku-ku, Tokyo 162-8480, Japan; Tel.: +81-3-5369-7328; e-mail: inoue.t@waseda.jp

**Keywords:** Sonic hedgehog (SHH), astrocyte, calcium oscillation, ATP, Smoothened (SMO), Smoothened agonist (SAG), cyclic AMP (cAMP), G protein, ATP-permeable channel

## ABSTRACT

Sonic hedgehog (SHH) is important for organogenesis during development. Recent studies have indicated that SHH is also involved in the proliferation and transformation of astrocytes to the reactive phenotype. However, the mechanisms underlying these are unknown. Involvement of SHH signaling in calcium (Ca) signaling has not been extensively studied. Here, we report that SHH and Smoothened agonist (SAG), an activator of the signaling receptor Smoothened (SMO) in the SHH pathway, activate Ca oscillations in cultured murine hippocampal astrocytes. The response was rapid, on a minute timescale, indicating a non-canonical pathway activity. Pertussis toxin blocked the SAG effect, indicating an involvement of a Gi coupled to SMO. Depletion of extracellular ATP by apyrase, an ATP degrading enzyme, inhibited the SAG-mediated activation of Ca oscillations. These results indicate that SAG increases

extracellular ATP levels by activating ATP release from astrocytes, resulting in Ca oscillation activation. We hypothesize that SHH activates SMO-coupled Gi in astrocytes, causing ATP release and activation of $G_{q/11}$-coupled P2 receptors on the same cell or surrounding astrocytes. Transcription factor activities are often modulated by Ca patterns; therefore, SHH signaling may trigger changes in astrocytes by activating Ca oscillations. This enhancement of Ca oscillations by SHH signaling may occur in astrocytes in the brain *in vivo* because we also observed it in hippocampal brain slices. In summary, SHH and SAG enhance Ca oscillations in hippocampal astrocytes, Gi mediates SAG-induced Ca oscillations downstream of SMO, and ATP-permeable channels may promote the ATP release that activates Ca oscillations in astrocytes.

## Introduction

Astrocytes are a major glial cell population in the central nervous system (CNS) with important roles in brain homeostasis, such as clearance of glutamate and GABA from the extracellular space, provision of nutrients from blood vessels to neurons, and control of extracellular pH (1, 2). Astrocytes are transformed into reactive astrocytes in response to brain injury and inflammation. Reactive astrocytes have altered gene expression patterns and morphology and play roles in scar formation and in preventing the spread of inflammation. Astrocytes also modulate neural excitability and synaptic connectivity by releasing so-called gliotransmitters, among which glutamate and ATP are major components (3, 4).

### *Sonic hedgehog*

The *Hedgehog* gene was identified in the 1970s as a gene involved in *Drosophila* larval segmentation (5). There are three *Hedgehog* homologs in vertebrates, Sonic hedgehog (*Shh*), Desert hedgehog (*Dhh*) and Indian hedgehog (*Ihh*) (6). *Shh* is involved in organogenesis and development of the CNS and is expressed throughout the body. In the absence of SHH, an SHH receptor, Patched, keeps a seven transmembrane receptor, Smoothened (SMO), from activating a transcription factor, GLI. Binding of SHH to Patched releases SMO to activate GLI, which translocates into the nucleus and activates transcription, thereby promoting cell proliferation and differentiation (7–9). Aside from this well-known canonical pathway, non-canonical pathways triggered by Patched activation have also been reported (10, 11). These pathways are not linked to GLI activation but regulate cell death (12), axon guidance (13), and cytoskeleton (14) with or without SMO activation.

### *SHH in the CNS*

In early CNS development, SHH is secreted from the notochord and floor plate as a morphogen to direct dorso-ventral patterning of the CNS. During late CNS development, SHH is found in the cerebral cortex, optic tectum and cerebellar cortex (15). SHH is also expressed in the adult CNS (16); SHH and Patched are expressed in the forebrain, cerebellar Purkinje cells and spinal cord motor neurons. SMO is expressed in circumventricular organs, granular cells in the hippocampal dentate gyrus and neurons in the reticular thalamic nuclei (17). The expression of SHH is particularly strong in the hippocampal dentate gyrus and the subventricular zone where adult neurogenesis takes place and retention, proliferation and differentiation of neural stem cells occurs (16). In hippocampal neurons, SHH is present presynaptically and postsynaptically (18), and Patched and SMO are localized not only in cell bodies but also in dendrites and postsynapses (19). Involvement of SHH in synaptic plasticity was also reported (20). *SHH* expression is activated upon traumatic injury in the brain (21, 22) including in astrocytes (21, 23). During injury, released

SHH increases the expression of glial fibrillary acidic protein (GFAP) in astrocytes and induces transformation of astrocytes to reactive astrocytes. SHH administration also induces transformation to reactive astrocytes (24, 25) and gliotransmitter release from astrocytes. All of these observations indicate important roles of SHH in the regulation of astrocytes. However, detailed mechanisms for these actions have not been elucidated.

### *Ca oscillation in glia*

While neurons communicate with each other by electrical activity, astrocytes transmit information by changing intracellular $Ca^{2+}$. Ca oscillation is frequently observed in astrocytes, in which Ca transients repeatedly occur in individual cells. These changing Ca patterns sometimes display wave-like propagation among astrocytes, which is called the Ca wave (26, 27). Various extracellular stimuli evoke Ca oscillations in astrocytes through various plasma membrane receptors, while intracellular Ca release occurs from the endoplasmic reticulum (ER) through inositol trisphosphate receptors (IP3Rs) downstream of $G_{q/11}$ coupled receptors .

ATP is a well-known stimulant that causes Ca oscillations in astrocytes. A class of ATP receptor, P2 receptors, namely P2X1/2/3/4/5/7 and P2Y1/2/4/6/12/13/14, is expressed in astrocytes (28). ATP-evoked Ca oscillation in astrocytes is not prevented by extracellular $Ca^{2+}$ removal; therefore, involvement of intracellular Ca release from IP3R downstream of $G_{q/11}$-coupled P2Y receptors is postulated (28).

ATP is released from astrocytes as a gliotransmitter and influences neuronal excitability (3, 4) and regulates Ca dynamics in astrocytes (29). Okuda et al. reported that SHH-stimulated astrocytes release ATP (30). Two mechanisms for releasing ATP from astrocytes are known: vesicular release and release through channels. Supporting vesicular release, a vesicular nucleotide transporter is expressed in astrocytes. For release through channels, ATP-permeable channels, maxi-anion channels, connexin hemichannels, pannexin hemichannels, and the P2X7 receptor are postulated to be involved. Several studies have shown that deprivation of oxygen and glucose, osmotic stimulation, and stretch stimulation induce ATP release from astrocytes through channels on the plasma membrane.

### *Aims of this study*

The high levels of SHH and related proteins in the adult hippocampus together with the inferred roles of SHH signaling in adult neurogenesis and brain injury led us to characterize cellular responses to SHH in cultured hippocampal cells. We found the enhancement of Ca oscillations in astrocytes within several min after application of SHH pathway agonists, namely SHH and Smoothened agonist (SAG). This enhancement was blocked by inhibition of Gi and removal of extracellular ATP. Together with other lines of evidence, we propose that the enhancement of Ca oscillations in astrocytes is initiated by the activation of SMO-coupled Gi, which leads to ATP release through ATP-permeable channels. This released ATP then enhances Ca oscillations in nearby astrocytes. We also observed enhanced Ca oscillations in astrocytes in brain slices; therefore, this mechanism may be functional in the *in vivo* brain as well.

## RESULTS

### *SHH and SAG evoke Ca oscillations in mouse hippocampal cultures*

Calcium imaging was performed by loading cultured mouse hippocampal cells with Fura-2 (Fig. 1A). Primary cultures of mouse hippocampal cells were exposed to SHH (500 pM, 10 ng/ml) in the presence of 1 μM

tetrodotoxin (TTX), and some of the cells exhibited spontaneous Ca oscillations before the agonist application. Addition of SHH evoked Ca oscillations in quiescent cells and enhanced the frequency of Ca oscillations in cells that had already shown spontaneous Ca oscillations before the agonist application (Fig. 1B): cumulative histogram during the agonist application periods was right-shifted from that during the baseline period (Fig. 1Bb; $p < 0.001$), indicating an increase in Ca oscillation frequency by SHH. A SMO agonist, SAG (5 μM), induced a similar increase in Ca oscillation frequency (Fig. 1C; $p < 0.001$). A series of different SHH and SAG concentrations resulted in increased or decreased Ca oscillation frequencies, but did not follow simple dose-response relationships (Figs. 1Bb, 1Cb and S1). Agonist-induced Ca frequency increase was evaluated by subtracting the baseline Ca frequency from that after the drug application in each cell (ΔFrequency). ΔFrequencies of cells applied with concentrations of SHH or SAG were compared to that of vehicle-applied control cells (0.1% DMSO; Fig. 1D–E). SHH increased Ca oscillation frequency significantly at 500 pM ($p < 0.001$) but less at 50 pM ($p < 0.01$) and not at 5 nM ($p = 0.82$). SAG increased Ca event frequency significantly at 5 μM ($p < 0.01$) and 50 nM ($p < 0.01$), and decreased the Ca event frequency at 500 nM ($p < 0.05$) and 100 nM ($p < 0.001$). SAG at 1 μM did not show difference from the control ($p = 0.31$). We used SHH at 500 pM hereafter. For SAG, we considered that 5 μM would produce the most reliable results because 100 nM SAG showed a large decrease in Ca oscillation frequency (Fig. S1F). The SAG concentration used hereafter was, therefore, 5 μM unless otherwise indicated. Some cells that did not show Ca transients during the initial 10 min baseline period started showing Ca transients after SHH or SAG stimulation; therefore, the stimuli increased the proportion of cells showing Ca transients as well as the frequency of Ca oscillations in each cell. About half of the cells did not show Ca transients throughout the recording period.

We tested cyclopamine (CPN), which is widely used as a SMO antagonist (31), on the assumption that it would block the effect of SAG. However, administration of CPN *per se* caused an increase in Ca oscillation frequency to a similar extent as SAG, and the addition of SAG to CPN further enhanced Ca oscillation frequency (Fig. 2Aa-b; $p < 0.001$ for base vs. CPN and base vs. CPN + SAG, respectively), which concealed the effect of subsequently applied SAG. ΔFrequencies of Ca oscillation both in the CPN and CPN + SAG periods were significantly larger than that of a control cell group (Fig. 2Ac; $p < 0.001$, respectively). CPN seemed to act as an agonist on the Ca oscillation enhancement mechanism originating from SMO. Such an agonistic action of CPN on a non-canonical SHH pathway has been previously reported (32, 33); therefore, we consider that the enhancement of Ca oscillations observed in this study was derived from the activation of a non-canonical SHH signaling pathway.

### *The SAG induced Ca oscillations are mediated by extracellular ATP*

We next investigated whether extracellular ATP is involved in the enhancement of Ca oscillations by SHH signaling because ATP is a well-known activator of Ca oscillations in astrocytes (34, 35). Administration of apyrase, an ATP degrading enzyme, to the extracellular space abolished the enhanced Ca oscillations evoked by SAG (Fig. 2Bb; $p < 0.001$ for base vs. SAG and $p < 0.05$ for SAG vs. apyrase), which was also shown in the ΔFrequency analysis (Fig. 2Bc; $p < 0.001$). This result indicates that SMO activation induced the increase in extracellular ATP, which then

enhanced Ca oscillations in the hippocampal cells. In a control experiment, a vehicle solution, HEPES-buffered saline (HBS) containing TTX, was added instead of apyrase, which produced an enhancement of Ca oscillation frequency (Fig. 2Ca; $p < 0.001$). ΔFrequency[(SAG + vehicle) – base] was greater than ΔFrequency(SAG – base) (Fig2Cb; $p < 0.001$). We have no clear explanation for this, but the dilution of SAG could be a cause because a relatively low concentration of SAG (50 nM) was as effective as 5 μM (Fig. 1E).

### *Astrocytes are responsible for the enhancement of Ca oscillations*

Primary hippocampal cell cultures are heterogeneous, containing neurons, astrocytes, microglia, oligodendrocytes, and other cell types. We, therefore, identified the cell types relevant to SAG-enhanced Ca oscillation. We assessed cell types in the hippocampal culture by immunohistochemistry with anti-MAP2, anti-S100β, anti-Iba1, and anti-Olig2 antibodies, which are markers for neurons, astrocytes, microglia and oligodendrocytes, respectively (Fig. S2). MAP2- and S100β-positive cells were observed throughout cultures (Fig. S2A and B). Iba1-positive cells were only found in one batch (10–20 cells in each coverslip culture) out of three culture batches (Fig. S2C). Olig2-positive cells were only found where neuron density was very high, but not in fields of view where neuron density was modest; we used such fields of view with modest neuron density for Ca imaging (Fig. S2D). Next, we performed Ca imaging followed by immunohistochemistry with anti-MAP2 and S100β antibodies (Fig. 3A). All the Fura-2-loaded cells were stained with either MAP2 or S100β in three fields of view from different cultures. S100β-positive cells were 58.9 ± 9.8% of all cells and the remainder were all MAP2-positive (n = 3 cultures). Ca transients were observed in 69.6 ± 14.1% of the S100β-positive cells and 32.5 ± 16.0% of the MAP2-positive cells. In our cultures, neurons showed frequent Ca transients in a synchronized fashion unless TTX was included in the bath solution (data not shown), but neurons showed far fewer spontaneous Ca transients than astrocytes when action potential generation was blocked by TTX. From these results, we consider that the major cell population that showed Ca oscillations was astrocytes. We tested whether the enhancement of Ca oscillations by SHH or SAG could be evoked in astrocyte cultures as well as in the primary heterogeneous culture, and this was indeed the case: the enhancing effects of SHH or SAG on Ca oscillation frequency were observed in the astrocyte culture (Fig. 3Bc; $p < 0.001$, and Fig 3Cb; $p < 0.001$, respectively). ΔFrequency of SHH and SAG compared with a DMSO (0.1%) applied control cell group showed increased Ca oscillation frequency with SHH or SAG (Fig. 3D; $p < 0.01$ and $p < 0.001$, respectively). We performed immunostaining of the astrocyte culture with the same antibodies as above. The anti-S100β antibody labeled cells over entire coverslips from two culture batches. However, no signals for anti-MAP2, anti-Iba1, and anti-Olig2 antibodies were observed (data not shown). Thus, it was clear that astrocytes were activated by SHH or SAG and showed enhanced Ca oscillations, although there is a possibility that neurons could also receive SHH or SAG and activate astrocyte Ca oscillations. To eliminate the possibility of astrocyte activation by neurons, we used astrocyte cultures in the following experiments.

### *Ca release from ER is necessary for Ca oscillations*

To characterize the mechanism of SAG-enhanced Ca oscillations, the source of $Ca^{2+}$ was investigated. Removal of $Ca^{2+}$ from the

extracellular solution did not alter the SAG- or SHH- induced enhancement of Ca oscillations in astrocytes (Figs. 4A and S3A, respectively): SAG enhanced Ca oscillation frequency with Ca-free medium (Fig. 4Ab; $p < 0.05$), and ΔFrequency(SAG – base) in Ca-free medium showed apparent difference from that of a control cell group (Fig. 4Ac; $p < 0.001$). In contrast, disruption of intracellular Ca release mechanisms resulted in drastic changes: 2-aminoethyl diphenylborinate (2-APB, 50 μM), an IP3R inhibitor, and thapsigargin (Tg, 100 nM), an inhibitor of the ER Ca-ATPase (36), blocked the SAG-induced enhancement of Ca oscillations (Fig. 4B-C). SAG did not take effect under 2-APB (Fig. 4Bb; base vs. 2-APB: $p = 0.38$; base vs. SAG: $p = 0.63$; 2-APB vs. SAG: $p = 0.70$), and ΔFrequency analysis comparing with a control cell group to which a vehicle solution containing only dimethyl sulfoxide (DMSO) was applied in place of 2-APB showed an apparent block of the SAG-induced Ca oscillation enhancement by 2-APB (Fig. 4Bc; ΔFrequency[(2-APB + SAG) – base] vs. ΔFrequency[(DMSO + SAG) – base]: $p < 0.001$). The SHH-induced enhancement of Ca oscillations was also blocked by 2-APB (Fig. S3B). Although 2-APB also blocks transient receptor potential (TRP) channels on the plasma membrane (37), we consider that the result with 2-APB was not due to TRP blockade because removal of extracellular $Ca^{2+}$ did not have an effect. Tg induced a slow increase in intracellular $Ca^{2+}$ concentration ($[Ca^{2+}]_i$) over 15 min. The level then decreased to the original baseline level. This is usually seen because of inhibited uptake of cytosolic $Ca^{2+}$ into ER. Ca oscillations occurred riding on the slow Tg -induced $[Ca^{2+}]_i$ increase, but the frequency was not increased by SAG (Fig. 4Cb), and ΔFrequency compared with the control cell group shows an apparent block of the SAG-induced Ca oscillation enhancement by Tg (ΔFrequency [(Tg + SAG) – base] vs. ΔFrequency[(DMSO + SAG) – base]: $p < 0.001$). Application of dantrolene (10 μM), which inhibits ryanodine receptor-mediated Ca release from ER, did not result in a clear inhibition of the SAG-enhanced Ca oscillations: SAG further enhanced the Ca oscillation frequency which had been enhanced by dantrolene (Fig. 4Db; base vs. dantrolene: $p < 0.001$, dantrolene vs. dantrolene + SAG: $p < 0.001$). ΔFrequency[(dantrolene + SAG) – base] almost overlapped with ΔFrequency[(DMSO + SAG) – base] (Fig. 4Dc). These results suggest that Ca release not though ryanodine receptor but through IP3Rs is relevant to the Ca oscillations enhanced by SAG.

### *SMO is coupled to Gi*

SMO is a seven transmembrane receptor that couples with a trimeric G protein, Gi (38, 39). We tested if the SMO enhancement of Ca oscillations requires Gi activation by incubating astrocytes with pertussis toxin (PTX), a Gi inhibitor. SAG induced an enhancement of Ca oscillations in PTX-treated astrocytes (Fig. 5Ab; $p < 0.001$), but it was significantly smaller than the SAG-induced enhancement without PTX-treatment. Furthermore, the addition of DMSO (0.1%) in place of SAG in PTX-treated astrocytes induced even larger increase in Ca oscillation frequency than that produced by SAG in PTX-treated astrocytes (Fig. 5Ac; $p < 0.001$). ΔFrequency analysis shows that the SAG-induced increase in Ca event frequency in the PTX treated cells was smaller than that by DMSO in PTX treated cells (Fig. 5Ad; ΔFrequency(SAG – base in PTX) vs. ΔFrequency(DMSO – base in PTX): $p < 0.001$) and much smaller than that by SAG without PTX treatment (ΔFrequency(SAG – base in PTX) vs. ΔFrequency(SAG – base without PTX): $p < 0.001$). Thus, we concluded that the enhancement of Ca oscillations by SAG requires Gi activity. Gi suppresses cAMP production from ATP by inhibiting adenylate cyclase. We confirmed that Gi was actually activated by SAG stimulation by intracellular cAMP imaging using a fluorescent protein-based cAMP indicator, Flamindo2 (40). SAG stimulation increased the fluorescence intensity of Flamindo2 in

astrocytes (Fig. 5Bc) compared with a control cell group to which vehicle (0.1% DMSO) was applied in place of SAG ($p < 0.001$, two-way ANOVA), indicating that cAMP concentration was decreased. These results showed that SAG stimulation activated Gi, presumably via SMO, which is necessary for the downstream SAG-induced enhancement of Ca oscillations.

### *Blockers of ATP-release channels inhibit the enhancement of Ca oscillations*

We hypothesized that the SMO and Gi activation by SAG induced ATP release, which led to the increased extracellular ATP concentration. To test this, carbenoxolone (CBX; 100 μM) and 1-octanol (2 mM), blockers of connexin hemichannels (41, 42), gadolinium ($Gd^{3+}$, 50 μM), a blocker of maxi-anion channels (43), and Brilliant blue G (BBG; 1 μM), a blocker of P2X7 receptors (44), were applied to astrocytes. The SAG-induced enhancement of Ca oscillation frequency was completely suppressed by CBX, 1-octanol and $Gd^{3+}$ (Fig. 6A–C). CBX and 1-octanol induced slow Ca transients lasting 5-10 min. CBX induced Ca event frequency enhancement, which was then inhibited by the addition of SAG (Fig. 6Ab; base vs. CBX: $p<0.001$; CBX vs. CBX + SAG: $p < 0.001$). ΔFrequency analysis together with a vehicle-applied control cell group (Fig. 6Ac) shows an apparent inhibition of the CBX-induced Ca oscillation enhancement by SAG (Fig. 6Ac; ΔFrequency[(CBX + SAG) – base] vs. ΔFrequency[(DMSO + SAG) – base]: $p < 0.001$). 1-octanol and $Gd^{3+}$ did not affect the baseline Ca oscillation frequency, and SAG addition did not change Ca oscillation frequency (Fig. 6Bb, and Fig. 6Cb, respectively). ΔFrequency analyses of these experiments show an apparent block of the SAG-induced Ca oscillation enhancement by 1-octanol (Fig. 6Cc; ΔFrequency[(1-octanol + SAG) - base] vs. ΔFrequency[(DMSO + SAG) - base]: $p < 0.001$) and $Gd^{3+}$ (Fig. 6Dc; ΔFrequency[($Gd^{3+}$ + SAG) - base] vs. ΔFrequency[(DMSO + SAG) - base]: $p < 0.001$). Under BBG, SAG increased Ca oscillation frequency (Fig. 6Db; BBG vs. BBG + SAG: $p < 0.001$). There was no statistical difference between ΔFrequency [(BBG + SAG) - base] and a control, ΔFrequency[(DMSO + SAG) - base] ($p = 0.16$). A concentration of 1 μM BBG blocks most P2X7 activity (44); therefore, P2X7 activity may not play a key role in the SAG-induced enhancement of Ca frequency. These results raise the possibility that astrocytes release ATP in response to SAG stimulation through maxi-anion channels and/or connexin hemichannels.

### *Ca oscillations in brain slice astrocytes are enhanced by SAG*

Astrocytes in culture have different features to those in the brain, e.g. in morphology and proliferation state (45). To test if the enhancement of Ca oscillations by SHH pathway activation is an atypical phenomenon in cultured astrocytes or a general feature of astrocytes, we performed Ca imaging in astrocytes in hippocampal slices. $[Ca^{2+}]_i$ in astrocytes labeled with SR101 (46) was monitored with a Ca dye, Fluo-4 (Fig. 7). In dentate gyrus of hippocampus, intensively stained cells with SR101 were found in molecular layer and weakly stained cells in granule cell layer. Cell bodies of some interneuron species are known to exist in inner molecular layer (47–49), and we indeed observed NeuN-positive, a general neuron marker, cell bodies in inner molecular layer: some in the proximity to granule cell layer and much fewer distant from granule cell layer (Fig. S4). Therefore, ROIs were placed on SR101 and Fluo-4 double positive cells in

molecular layer excluding cells within 30 µm from granule cell layer, where most, not to say all, SR101-positive cells should be astrocytes. During the baseline period, some astrocytes showed Ca oscillations, and SAG (50 nM) enhanced Ca oscillation frequency (Fig. 7C; $p < 0.01$), while vehicle (0.1% DMSO) did not (Fig. 7B; $p = 0.45$). ΔFrequency analysis also showed a significant difference between SAG and vehicle (Fig. 7D; $p < 0.01$). This result indicates that the enhancement of Ca oscillations by SHH signaling operates not only in cultured astrocytes but also in brain slice astrocytes.

## DISCUSSION

Astrocytes are known to respond to stimuli by evoking or altering their Ca oscillation patterns (29, 50, 51), in which $Gq_{/11}$-coupled receptors, namely metabotropic glutamate receptors and P2Y receptors are often involved (52–54). In this study, the enhancement of Ca oscillations by SAG was inhibited by the degradation of extracellular ATP with apyrase or inhibition of Gi with PTX. Therefore, the enhancement of Ca oscillations did not result from direct activation of $Gq_{/11}$ but from Gi activation by SMO, which in turn evoked ATP release. ATP release from astrocytes by SHH has been previously reported (30). The increased extracellular ATP may have activated P2Y receptors in adjacent astrocytes, and possibly in the astrocytes that released ATP, thereby enhancing the Ca oscillations in these cells. P2Y1/2/4/6/12/13/14 receptors are expressed in astrocytes, and P2Y1/2/4/6 receptors are coupled with $Gq_{/11}$ (52, 55).

The finding that CBX, 1-octanol, and $Gd^{3+}$ inhibited the enhancement of Ca oscillations by SAG raises the possibility that the ATP release downstream of activated SMO was not mediated by a vesicular release mechanism but through ATP-permeable channels, namely connexin hemichannels and maxi-anion channels, which are sensitive to these antagonists. SLCO2A1 is a core component of the maxi-anion channel (56), although the precise molecular composition of the maxi-anion channel is still unclear (57). G protein-coupled receptor activation (58) and dephosphorylation of maxi-anion channels (59) are involved in the opening mechanisms. The presumed suppression of cAMP-dependent protein kinase (PKA) downstream of Gi activation by SAG could lead to dephosphorylation of maxi-anion channels. The opening mechanism of connexin hemichannels has not been clarified, and thus the mechanisms underlying ATP release through them are unknown (60). However, because both CBX and $Gd^{3+}$ block a wide range of channels (61), they could directly inhibit the Ca oscillation mechanism downstream of ATP release rather than affecting the ATP release channels. Furthermore, 2-APB inhibits connexin channels with varying potencies depending on the subunit (62). Thus, an alteration of connexin-mediated ATP release by 2-APB could also be involved in the 2-APB inhibition of the SAG-induced Ca oscillation enhancement (Fig. 4) in addition to the inhibition of IP3R by 2-APB. Characterization of the ATP-release mechanisms downstream of SMO in astrocytes remains to be elucidated.

The lag in the onset of changes in the frequency of Ca transient on application of SHH or SAG varied considerably among cells. In some cells the increase started within 1 min and in others responses started after delays of 2-5 min. This variability indicates that some of the steps from SMO activation to the increase in extracellular ATP concentration are slow with variable speeds among cells. Extracellular ATP accumulation is one such variable step. The not-so-simple dose-response in Ca oscillation frequency in response to SHH or SAG (Fig. 1D and E) may reflect such a complicated mechanism, together with a possibility that SHH and SAG have multiple sites of action on their receptors.

Although we consider that the direct ATP release and subsequent Ca oscillations was via a non-canonical SHH pathway through Gi

activation, the canonical SHH pathway, in which GLI is activated and transported to the nucleus, may be influenced by the non-canonical series of events. When the SHH signal is turned off, GLI is ubiquitinated by β-TrPC, which is induced by the activities of PKA, GSK3β, and CK1. This removes the GLI active domain and keeps GLI inactive (9). When the SHH signal is turned on, GLI escapes from ubiquitination, and full-length GLI dissociates from the negative regulator, Suppressor of Fused (SuFu), and migrates into the nucleus (9, 63, 64). Although the complex interactions between SMO and GLI are not understood in detail, several lines of evidence indicate that PKA is a key negative regulator of the canonical SHH signal downstream of SMO (65–69). Thus, the presumed PKA deactivation following Gi activation and the decrease in cAMP concentration, which were confirmed in this study, may reduce the negative effect of PKA and push the balance of inactive/active GLI molecules to the active side. Whether this deactivation of PKA by activation of Gi downstream of SMO is peculiar to astrocytes or a more general feature needs to be clarified.

Adenylyl cyclase 5 and 6 (AC5/6) localize to primary cilia (70) and are sensitive to $[Ca^{2+}]_i$ (71). SHH and SAG raise $[Ca^{2+}]_i$ in primary cilia, possibly via Trp channels and $Gd^{3+}$-sensitive plasma membrane channels (72–74). Moore et al. reported that cAMP concentration in primary cilia is five-fold higher than that of the level in whole-cells, and SHH stimulation increased ciliary $[Ca^{2+}]_i$ and decreased ciliary cAMP concentration in mouse embryonic fibroblasts (74). They suggested that inhibition of AC5/6 by $Ca^{2+}$ is the mechanism for the reduction of cAMP in cilia by SHH. Primary cilia may behave as isolated compartments where concentration and dynamics of signaling molecules, including $Ca^{2+}$, are separate from global cytoplasmic $Ca^{2+}$ (73, 75). Therefore, the Ca increase and cAMP reduction observed in this study may have occurred in SAG-stimulated primary cilia of astrocytes in parallel with the global enhancement of cytoplasmic Ca oscillations and reduced concentrations of cAMP.

In the adult brain, SHH is secreted upon brain injury and makes astrocytes reactive (21, 25). In severe cases, the gathered astrocytes then form a characteristic astrocyte scar around the injured site (76, 77). Although the intercellular and intracellular signaling mechanisms that make astrocytes reactive and form scars are not well characterized, an increase in extracellular ATP has been implicated in the initial microglial activation (78), leading to transformation of astrocytes to the reactive state (79). Although it is proposed that ATP is released from injured cells as "find me" (80) or "eat me" (81) signals, intact astrocytes could be involved in the increase in extracellular ATP in the early phase of the response to injury by responding to SHH release because SHH levels are raised after traumatic brain injury (21, 22). SHH is also expressed after brain ischemia (82), and administration of SHH to rats just after stroke partially relieves neurological damage with improved angiogenesis and neuron survival (83). The release of ATP from astrocytes and enhancement of Ca oscillations in astrocytes may also be involved in recovery from brain ischemia.

Ca oscillations are observed in a wide range of cell types (51), and controls various vital functions of cells, e.g. egg activation in fertilization (84) and differentiation of osteoclasts (85). However, outcomes of many Ca oscillation events are not known, including for the Ca oscillations in astrocytes. A possible scenario is that Ca oscillations activate Ca-dependent transcription factors and alters gene expression patterns, which may modulate cellular proliferation, differentiation and programmed cell death. It was proposed that different sets of transcription factors are activated according to the frequency and amplitude of Ca oscillations following experiments in which intracellular Ca patterns were artificially controlled (86, 87). Nuclear factor of activated T cells (NFAT) activity is controlled by Ca oscillations (86–88), and dephosphorylation of NFAT by calcineurin, a Ca-dependent phosphatase, is postulated as a mechanism for NFAT activation by Ca oscillations (89). It is conceivable that the activity of GLI via the canonical SHH

pathway is regulated by Ca oscillations evoked through a non-canonical pathway, because the activity of GLI is controlled by dephosphorylation (68). The expression of SHH is increased during development and upon traumatic injury; therefore, the Ca oscillations in astrocytes observed in this study may play roles in differentiation and activation of astrocytes and may affect nearby neurons by releasing gliotransmitters. In future research, it will be of great interest to determine the outcome of Ca oscillations induced by SHH in slice preparations or *in vivo*.

In Summary, we found that [1] Ca oscillations in the hippocampus were enhanced in astrocytes in response to SHH or SAG; [2] the enhancement of Ca oscillations by SAG required IP3R-dependent Ca release; [3] Gi plays a role downstream of SMO in the enhancement of Ca oscillations by SAG; [4] ATP-permeable channels may be responsible for the ATP release that activates Ca oscillations in surrounding astrocytes; [5] the enhancement of Ca oscillations by SHH signaling was not peculiar to cultured astrocytes and was also observed in slice preparations.

## EXPERIMENTAL PROCEDURES

### *Animal care*

Animal care was in accordance with guidelines outlined by the Institutional Animal Care and Use Committee of Waseda University. The protocol was approved by the Committee on the Ethics of Animal Experiments of Waseda University. All efforts were made to minimize the number of animals used and their suffering during experiments.

### *Cell culture*

Primary hippocampal cultures were prepared from E17 ICR mice as described previously (90) with modifications: hippocampi were dissociated with 0.25% papain (38N18758, Worthington, Lakewood, NJ, USA) containing 0.25% DNase in Glucose mix [phosphate-buffered saline (PBS) containing 0.4% glucose, 0.04% BSA and 0.04% L-cysteine] at 37°C for 5 min. Dissociated cells were seeded on poly-ethyleneimine (PEI)-coated round glass coverslips (12 mm in diameter, $1 \times 10^5$ cells/slip) with Neurobasal medium (12349-015, Thermo Fisher Scientific, Tokyo, Japan) containing 2% B-27 supplement (Thermo Fisher Scientific), 1% L-glutamine and 0.05% penicillin-streptomycin. Cells kept *in vitro* for 11-17 days were used. The culture confluency was 80–90%.

Hippocampal astrocyte cultures were prepared from E17 ICR mice as described previously (91) with modifications: dissociated cells were plated in PEI-coated 75 $cm^2$ culture flasks ($15 \times 10^6$ cells/10 ml) in DMEM/F12 medium (Sigma-Aldrich, Tokyo, Japan) containing 5% horse serum and 5% fetal bovine serum, 0.5% L-glutamine and 0.36% penicillin-streptomycin. After 10 days in culture, the cells were suspended with 0.025% trypsin in Hanks' balanced salt solution, $Ca^{2+}$ and $Mg^{2+}$ free, and plated on PEI-coated round glass coverslips (12 mm in diameter, $5 \times 10^4$ cells/slip) with the same culture medium. Cultures at 80–90% confluency were used for imaging.

### *Immunohistochemistry*

Cells were fixed in 4% paraformaldehyde in PBS for 15 min, permeabilized with 0.25% Triton X-100 in PBS for 10 min and blocked with 1% BSA for 1 h at room temperature (RT). Cells were incubated overnight at 4°C with the primary antibody and for 1 h at RT with the secondary antibody (1:1000). The primary antibodies used were: anti-MAP2 (1:500) (sc-20172, sc-32791, Santa Cruz Biotechnology, Dallas, TX, USA), anti-S100β (1:100) (sc-393919, Santa Cruz Biotechnology), anti-Iba1 (1:500) (019-19741, Fujifilm Wako Pure Chemical Corp., Osaka, Japan), and anti-Olig2 (1:500) (AB9610, Merck, Tokyo Japan). The secondary antibodies used were: Alexa

Fluor 488 donkey anti-mouse IgG (abcam, Tokyo, Japan) and Alexa Fluor 647 goat anti-rabbit IgG (Thermo Fisher Scientific, Tokyo, Japan). Cell nuclei were stained with DAPI (Santa Cruz Biotechnology).

*Reagents*

SAG (sc-212905, Santa Cruz Biotechnology, or S0224, KT Laboratories, St. Paul, MN, USA) was dissolved in DMSO (D2650, Sigma-Aldrich) at 5 mM and stored at -20°C. SHH (murine, 315-22-5UG, Peprotech, Rocky Hill, NJ, USA) was dissolved in PBS(+) and stored at -80°C in 100 µg/ml aliquots. 2-APB (D0281, Tokyo Chemical Industry, Tokyo, Japan) was dissolved in DMSO at 50 mM and stored at -20°C. PTX [516560, Calbiochem (Sigma-Aldrich)] was dissolved in $H_2O$ at 100 µg/ml, stored at 4°C, and used within 6 months. CBX (C4790, Sigma-Aldrich) was dissolved in DMSO at 100 mM and stored at -20°C. Gadolinium chloride (16506-71, Nacalai Tesque, Kyoto, Japan) was dissolved in $H_2O$ at 50 mM, stored at -20°C, and used within 10 days. 1-Octanol (25506-62, Nacalai Tesque) was dissolved in DMSO at 2 M and stored at -20°C. BBG (B1146, Tokyo Chemical Industry) was dissolved in DMSO at 1 mM and stored at -20°C.

*DNA transfection*

Cultured astrocytes were electroporated with plasmid DNA encoding Flamindo 2 (40) using the Amaxa Basic Nucleofector Kit for Primary Mammalian Glial Cells (Lonza Japan, Tokyo, Japan) according to the manufacturer's protocol. Nucleofected astrocytes were placed on PEI-coated round glass coverslips (12 mm in diameter, $1 \times 10^5$ cells/slip). After 1-2 hours, DMEM/F12 medium (Sigma-Aldrich) containing 5% horse serum, 5% fetal bovine serum, 0.5% L-glutamine and 0.36% penicillin-streptomycin was added. Two-five days after nucleofection 50-60% confluent cells were used.

*Cell culture imaging*

Coverslips holding cultured cells were mounted in a stainless steel chamber containing HBS (in mM, 20 HEPES, 115 NaCl, 5.4 KCl, 1 $MgCl_2$, 2 $CaCl_2$, 10 glucose, pH 7.4). A Ca indicator, Fura-2 was loaded into cells by incubation with 2.5 µM Fura-2-AM/HBS (Dojindo, Kumamoto, Japan) at 37°C for 10 min followed by three washes with HBS. TTX (1 µM) was added to HBS throughout the imaging procedures (HBS-TTX) when primary culture preparations were used to avoid Ca events evoked by neuronal activities. Time-lapse imaging was performed with an inverted microscope (IX71, Olympus, Tokyo, Japan) with a 20× objective (UApo/340, N.A., 0.75, Olympus). Fura-2 was excited by 340 and 380 nm wavelength light alternating every 3 s and fluorescence was detected with a cooled CCD camera (ORCA-ER, Hamamatsu Photonics, Hamamatsu, Japan) through a beam splitter (400 nm) and an emission filter (420 nm long pass). The fluorescence intensity ratio ($F_{340}/F_{380}$) was calculated for each time point of each region of interest (ROI) by dividing fluorescence intensity excited by 340 nm light by that excited by 380 nm light after background subtraction. Fluorescence signals of each wavelength image were calculated by averaging pixel intensities in an oval ROI covering each cell body. ROIs were set on all cells identifiable by the Fura-2 staining in each field of view. Ca transients were detected by finding $F_{340}/F_{380}$ changes exceeding a threshold from a baseline value along the time course of the $F_{340}/F_{380}$ ratio. The baseline value for each time point of each ROI ($R_{base}$) was determined by calculating the average of the $F_{340}/F_{380}$ values of the ROI for 20 frames just before the time point. To reject large deflecting values due to Ca transients, data points with values twice larger than the standard deviation of the values of the ROI throughout the recording period were omitted from the baseline calculation. In experiments where the Ca recording baseline suffered from

artefactual slow drifts because of optical interference by applied reagents (Tg, 2-APB, CBX and 1-octanol; see Fig. 4 and 6), linear regression instead of averaging was used to determine $R_{base}$, which was effective to cancel slow baseline drift (Fig. S5). Cells showed various Ca changes in this study; from apparent large spikes of Ca transients to much smaller Ca changes just above the noise level. Because we focused on the former clear Ca transients in this study, we determined the threshold for detection of Ca events as 0.08 for cultured cells, which effectively isolated the clear Ca transients. In most of the Ca measurement experiments the frequencies of Ca transients before drug application (baseline) and after drug application periods were calculated in each cell. These frequencies of all cells from repeated experiments were pooled as a group, and are displayed by cumulative histograms in figures. To make the Ca frequency changes clearer, the baseline Ca event frequency was subtracted from the frequency after drug application in each cell (ΔFrequency). ΔFrequencies of all cells from repeated experiments were pooled as a group, and are displayed as cumulative histograms in figures and compared with other groups of different experimental conditions by considering the null hypothesis that ΔFrequency of cells is the same between different experimental conditions. When cAMP concentration was measured, Fura-2 was loaded into cultured astrocytes that had been transfected 2-5 days previously with plasmid encoding Flamindo 2, and time-lapse imaging of three alternating wavelengths was performed every 5 s, by adding a blue-excitation and a green emission acquisition for Flamindo 2 (490-500 nm excitation and 515-560 nm emission filters with a 505 nm beam splitter) to the Fura-2 dual wavelength acquisition described above. There was no detectable cross talk between the Fura-2 and Flamindo 2 optical paths. For time course analysis of Flamindo 2 results, the fluorescence signal of each frame was divided by that of the first image frame ($F/F_0$) after background subtraction. Image acquisition and data analysis were performed with custom-made TI Workbench software written by T. I. (92).

### *Brain slice*

Hippocampal slices, 400 μm thick, were prepared from 4-8-week-old male C57BL/6 mice using a standard method (93) and used within one day of preparation. A Ca indicator, Fluo-4 AM (Thermo Fisher Scientific), and an astrocyte marker, sulforhodamine 101 (SR101, sc-215929, Santa Cruz), were loaded onto the slices by incubating with 5 μM Fluo-4 AM in artificial cerebrospinal fluid (ACSF; in mM, 1 NaCl 125, KCl 2.5, $NaH_2PO_4$ 1.25, $NaHCO_3$ 26, $MgCl_2$ 1, $CaCl_2$ 2 and glucose 20, 310–315 mOsm and bubbled with a 95% $O_2$ and 5% $CO_2$ gas mixture) at 34°C for 40 min. SR101 (1 μM) was then added and the slices were stained for another 20 min. After staining, slices were transferred to ACSF and kept at RT for 30 min before the time-lapse imaging. Time-lapse imaging was performed with an in-house two-photon microscope (92) mounted on an upright microscope (BX51, Olympus) with a 20× water immersion objective (XLUMPlanFl, N.A., 0.95, Olympus). Brain slices were continuously superfused with ACSF containing 1 μM TTX at 34°C. An excitation laser of wavelength 920 nm (titanium-sapphire pulse laser, Mai Tai DeepSee, Spectra-Physics, Santa Clara, CA, USA) was used and the emission was divided with a 580 nm beam splitter and passed through a 495-540 or 575-630 nm band-pass filter for the Fluo-4 and the SR101 signals, respectively. Data analysis was performed as described for the cell culture experiments except that the ROIs were placed on SR101 and Fluo-4 double positive cells in the molecular layer and the Fluo-4 fluorescence

intensity of each ROI was normalized by dividing by that of the first image frame ($F/F_0$). A baseline value for each data point was calculated as described above by averaging the preceding 20 frames, and fluorescence intensity of the data point of the ROI was subtracted with the baseline value. We used 0.3 as the threshold to detect Ca transients. Although SR101 is widely used to stain astrocytes, hyperexcitation of neurons is a known side effect (94, 95). We consider that if this side effect occurred in this study it was minute because the concentration of SR101 used was much lower than the suggested threshold (between 50 and 250 μM) (95).

### *Statistics*

Mann-Whitney U-test included in the ALGLIB library (www.alglib.net) implemented in TI Workbench was used to compare two groups unless otherwise indicated. All indicated data are given as the average ± s.d.

## ACKNOWLEDGEMENTS

The authors thank Prof. N. Murata for statistical advice and Prof. K. Hanashima for gifts of antibodies. This work was supported by Grants-in-Aid for Scientific Research from the Japan Society for the Promotion of Science (TI: 23113515 and 23300121), the JSPS Core-to-Core Program, Advanced Research Networks (CA, TK and TI), the Private University Research Branding Project (MEXT, Japan, TI), and Waseda University Grants for Special Research Projects (TI).

## CONFLICT OF INTEREST

The authors declare that they have no conflicts of interest with the contents of this article.

## REFERENCES


1. Kimelberg, H. K., and Nedergaard, M. (2010) Functions of astrocytes and their potential as therapeutic targets. *Neurother. J. Am. Soc. Exp. Neurother.* **7**, 338–353
2. Voutsinos-Porche, B., Bonvento, G., Tanaka, K., Steiner, P., Welker, E., Chatton, J.-Y., Magistretti, P. J., and Pellerin, L. (2003) Glial glutamate transporters mediate a functional metabolic crosstalk between neurons and astrocytes in the mouse developing cortex. *Neuron*. **37**, 275–286
3. Butt, A. M. (2011) ATP: a ubiquitous gliotransmitter integrating neuron-glial networks. *Semin. Cell Dev. Biol.* **22**, 205–213
4. Parpura, V., and Zorec, R. (2010) Gliotransmission: Exocytotic release from astrocytes. *Brain Res. Rev.* **63**, 83–92
5. Nüsslein-Volhard, C., and Wieschaus, E. (1980) Mutations affecting segment number and polarity in Drosophila. *Nature*. **287**, 795–801
6. Echelard, Y., Epstein, D. J., St-Jacques, B., Shen, L., Mohler, J., McMahon, J. A., and McMahon, A. P. (1993) Sonic hedgehog, a member of a family of putative signaling molecules, is implicated in the regulation of CNS polarity. *Cell*. **75**, 1417–1430
7. Briscoe, J., and Thérond, P. P. (2013) The mechanisms of Hedgehog signalling and its roles in development and disease. *Nat. Rev. Mol. Cell Biol.* **14**, 416–429
8. Choudhry, Z., Rikani, A. A., Choudhry, A. M., Tariq, S., Zakaria, F., Asghar, M. W., Sarfraz, M. K., Haider, K., Shafiq, A. A., and Mobassarah, N. J. (2014) Sonic hedgehog signalling pathway: a complex network. *Ann. Neurosci.* **21**, 28–31
9. Sasai, N., and Briscoe, J. (2012) Primary cilia and graded Sonic Hedgehog signaling. *Wiley Interdiscip. Rev. Dev. Biol.* **1**, 753–772
10. Brennan, D., Chen, X., Cheng, L., Mahoney, M., and Riobo, N. A. (2012) Noncanonical Hedgehog signaling. *Vitam. Horm.* **88**, 55–72
11. Jenkins, D. (2009) Hedgehog signalling: emerging evidence for non-canonical pathways. *Cell. Signal.* **21**, 1023–1034
12. Chang, H., Li, Q., Moraes, R. C., Lewis, M. T., and Hamel, P. A. (2010) Activation of Erk by sonic hedgehog independent of canonical hedgehog signalling. *Int. J. Biochem. Cell Biol.* **42**, 1462–1471
13. Yam, P. T., Langlois, S. D., Morin, S., and Charron, F. (2009) Sonic hedgehog guides axons through a noncanonical, Src-family-kinase-dependent signaling pathway. *Neuron*. **62**, 349–362
14. Chinchilla, P., Xiao, L., Kazanietz, M. G., and Riobo, N. A. (2010) Hedgehog proteins activate pro-angiogenic responses in endothelial cells through non-canonical signaling pathways. *Cell Cycle Georget. Tex*. **9**, 570–579
15. Martí, E., and Bovolenta, P. (2002) Sonic hedgehog in CNS development: one signal, multiple outputs. *Trends Neurosci.* **25**, 89–96
16. Álvarez-Buylla, A., and Ihrie, R. A. (2014) Sonic hedgehog signaling in the postnatal brain. *Semin. Cell Dev. Biol.* **33**, 105–111
17. Traiffort, E., Charytoniuk, D., Watroba, L., Faure, H., Sales, N., and Ruat, M. (1999) Discrete localizations of hedgehog signalling components in the developing and adult rat nervous system. *Eur. J. Neurosci.* **11**, 3199–3214
18. Petralia, R. S., Wang, Y.-X., Mattson, M. P., and Yao, P. J. (2011) Sonic hedgehog distribution within mature hippocampal neurons. *Commun. Integr. Biol.* **4**, 775–

777
19. Petralia, R. S., Schwartz, C. M., Wang, Y.-X., Mattson, M. P., and Yao, P. J. (2011) Subcellular Localization of Patched and Smoothened, the Receptors for Sonic Hedgehog Signaling, in the Hippocampal Neuron. *J. Comp. Neurol.* **519**, 3684–3699
20. Yao, P. J., Petralia, R. S., and Mattson, M. P. (2016) Sonic Hedgehog Signaling and Hippocampal Neuroplasticity. *Trends Neurosci.* **39**, 840–850
21. Amankulor, N. M., Hambardzumyan, D., Pyonteck, S. M., Becher, O. J., Joyce, J. A., and Holland, E. C. (2009) Sonic hedgehog pathway activation is induced by acute brain injury and regulated by injury-related inflammation. *J. Neurosci.* **29**, 10299–10308
22. Lee, J. H., Chung, Y. C., Bok, E., Lee, H., Huh, S. H., Lee, J. E., Jin, B. K., and Ko, H. W. (2017) Injury-stimulated Sonic hedgehog expression in microglia contributes to neuroinflammatory response in the MPTP model of Parkinson's disease. *Biochem. Biophys. Res. Commun.* **482**, 980–986
23. Pitter, K. L., Tamagno, I., Feng, X., Ghosal, K., Amankulor, N., Holland, E. C., and Hambardzumyan, D. (2014) The SHH/Gli pathway is reactivated in reactive glia and drives proliferation in response to neurodegeneration-induced lesions. *Glia*. **62**, 1595–1607
24. Garcia, A. D. R., Petrova, R., Eng, L., and Joyner, A. L. (2010) Sonic hedgehog regulates discrete populations of astrocytes in the adult mouse forebrain. *J. Neurosci.* **30**, 13597–13608
25. Sirko, S., Behrendt, G., Johansson, P. A., Tripathi, P., Costa, M., Bek, S., Heinrich, C., Tiedt, S., Colak, D., Dichgans, M., Fischer, I. R., Plesnila, N., Staufenbiel, M., Haass, C., Snapyan, M., Saghatelyan, A., Tsai, L.-H., Fischer, A., Grobe, K., Dimou, L., and Götz, M. (2013) Reactive glia in the injured brain acquire stem cell properties in response to sonic hedgehog. *Cell Stem Cell*. **12**, 426–439
26. Scemes, E., and Giaume, C. (2006) Astrocyte calcium waves: What they are and what they do. *Glia*. **54**, 716–725
27. Pasti, L., Volterra, A., Pozzan, T., and Carmignoto, G. (1997) Intracellular Calcium Oscillations in Astrocytes: A Highly Plastic, Bidirectional Form of Communication between Neurons and Astrocytes In Situ. *J. Neurosci.* **17**, 7817–7830
28. Verkhratsky, A., Verkhrasky, A., Krishtal, O. A., and Burnstock, G. (2009) Purinoceptors on neuroglia. *Mol. Neurobiol.* **39**, 190–208
29. Hamilton, N., Vayro, S., Kirchhoff, F., Verkhratsky, A., Robbins, J., Gorecki, D. C., and Butt, A. M. (2008) Mechanisms of ATP- and glutamate-mediated calcium signaling in white matter astrocytes. *Glia*. **56**, 734–749
30. Okuda, H., Tatsumi, K., Morita-Takemura, S., Nakahara, K., Nochioka, K., Shinjo, T., Terada, Y., and Wanaka, A. (2016) Hedgehog Signaling Modulates the Release of Gliotransmitters from Cultured Cerebellar Astrocytes. *Neurochem. Res.* **41**, 278–289
31. Chen, J. K., Taipale, J., Young, K. E., Maiti, T., and Beachy, P. A. (2002) Small molecule modulation of Smoothened activity. *Proc. Natl. Acad. Sci.* **99**, 14071–14076
32. Rohatgi, R., Milenkovic, L., Corcoran, R. B., and Scott, M. P. (2009) Hedgehog signal transduction by Smoothened: pharmacologic evidence for a 2-step activation

process. *Proc. Natl. Acad. Sci. U. S. A.* **106**, 3196–3201
33. Teperino, R., Amann, S., Bayer, M., McGee, S. L., Loipetzberger, A., Connor, T., Jaeger, C., Kammerer, B., Winter, L., Wiche, G., Dalgaard, K., Selvaraj, M., Gaster, M., Lee-Young, R. S., Febbraio, M. A., Knauf, C., Cani, P. D., Aberger, F., Penninger, J. M., Pospisilik, J. A., and Esterbauer, H. (2012) Hedgehog partial agonism drives Warburg-like metabolism in muscle and brown fat. *Cell*. **151**, 414–426
34. Koizumi, S. (2010) Synchronization of $Ca^{2+}$ oscillations: involvement of ATP release in astrocytes. *FEBS J.* **277**, 286–292
35. Vishnu, N., Jadoon Khan, M., Karsten, F., Groschner, L. N., Waldeck-Weiermair, M., Rost, R., Hallström, S., Imamura, H., Graier, W. F., and Malli, R. (2014) ATP increases within the lumen of the endoplasmic reticulum upon intracellular $Ca^{2+}$ release. *Mol. Biol. Cell*. **25**, 368–379
36. Charles, A. C., Dirksen, E. R., Merrill, J. E., and Sanderson, M. J. (1993) Mechanisms of intercellular calcium signaling in glial cells studied with dantrolene and thapsigargin. *Glia*. **7**, 134–145
37. Bootman, M. D., Collins, T. J., Mackenzie, L., Roderick, H. L., Berridge, M. J., and Peppiatt, C. M. (2002) 2-Aminoethoxydiphenyl borate (2-APB) is a reliable blocker of store-operated $Ca^{2+}$ entry but an inconsistent inhibitor of InsP3-induced $Ca^{2+}$ release. *FASEB J.* **16**, 1145–1150
38. Ayers, K. L., and Thérond, P. P. (2010) Evaluating Smoothened as a G-protein-coupled receptor for Hedgehog signalling. *Trends Cell Biol.* **20**, 287–298
39. Mukhopadhyay, S., and Rohatgi, R. (2014) G-protein-coupled receptors, Hedgehog signaling and primary cilia. *Semin. Cell Dev. Biol.* **33**, 63–72
40. Odaka, H., Arai, S., Inoue, T., and Kitaguchi, T. (2014) Genetically-Encoded Yellow Fluorescent cAMP Indicator with an Expanded Dynamic Range for Dual-Color Imaging. *PLOS ONE*. **9**, e100252
41. Murana, E., Pagani, F., Basilico, B., Sundukova, M., Batti, L., Angelantonio, S. D., Cortese, B., Grimaldi, A., Francioso, A., Heppenstall, P., Bregestovski, P., Limatola, C., and Ragozzino, D. (2017) ATP release during cell swelling activates a $Ca^{2+}$ -dependent $Cl^{-}$ current by autocrine mechanism in mouse hippocampal microglia. *Sci. Rep.* **7**, 4184
42. Yin, X., Feng, L., Ma, D., Yin, P., Wang, X., Hou, S., Hao, Y., Zhang, J., Xin, M., and Feng, J. (2018) Roles of astrocytic connexin-43, hemichannels, and gap junctions in oxygen-glucose deprivation/reperfusion injury induced neuroinflammation and the possible regulatory mechanisms of salvianolic acid B and carbenoxolone. *J. Neuroinflammation*. **15**, 97
43. Liu, H.-T., Toychiev, A. H., Takahashi, N., Sabirov, R. Z., and Okada, Y. (2008) Maxi-anion channel as a candidate pathway for osmosensitive ATP release from mouse astrocytes in primary culture. *Cell Res.* **18**, 558–565
44. Jiang, L. H., Mackenzie, A. B., North, R. A., and Surprenant, A. (2000) Brilliant blue G selectively blocks ATP-gated rat $P2X_7$ receptors. *Mol. Pharmacol.* **58**, 82–88
45. Lange, S. C., Bak, L. K., Waagepetersen, H. S., Schousboe, A., and Norenberg, M. D. (2012) Primary cultures of astrocytes: their value in understanding astrocytes in health and disease. *Neurochem. Res.* **37**, 2569–2588
46. Nimmerjahn, A., Kirchhoff, F., Kerr, J. N. D., and Helmchen, F. (2004)

Sulforhodamine 101 as a specific marker of astroglia in the neocortex in vivo. *Nat. Methods*. **1**, 31–37
47. Williams, P. A., Larimer, P., Gao, Y., and Strowbridge, B. W. (2007) Semilunar granule cells: glutamatergic neurons in the rat dentate gyrus with axon collaterals in the inner molecular layer. *J. Neurosci.* **27**, 13756–13761
48. Freund, T. F., and Buzsáki, G. (1996) Interneurons of the hippocampus. *Hippocampus*. **6**, 347–470
49. Hajos, N., Acsady, L., and Freund, T. F. (1996) Target selectivity and neurochemical characteristics of VIP-immunoreactive interneurons in the rat dentate gyrus. *Eur. J. Neurosci.* **8**, 1415–1431
50. Mariotti, L., Losi, G., Sessolo, M., Marcon, I., and Carmignoto, G. (2016) The inhibitory neurotransmitter GABA evokes long-lasting $Ca^{2+}$ oscillations in cortical astrocytes. *Glia*. **64**, 363–373
51. Tsien, R. W., and Tsien, R. Y. (1990) Calcium channels, stores, and oscillations. *Annu. Rev. Cell Biol.* **6**, 715–760
52. Abbracchio, M. P., and Ceruti, S. (2006) Roles of P2 receptors in glial cells: focus on astrocytes. *Purinergic Signal.* **2**, 595–604
53. James, G., and Butt, A. M. (2001) P2X and P2Y purinoreceptors mediate ATP-evoked calcium signalling in optic nerve glia in situ. *Cell Calcium*. **30**, 251–259
54. Salter, M. W., and Hicks, J. L. (1994) ATP-evoked increases in intracellular calcium in neurons and glia from the dorsal spinal cord. *J. Neurosci.* **14**, 1563–1575
55. Burnstock, G. (2008) Purinergic signalling and disorders of the central nervous system. *Nat. Rev. Drug Discov.* **7**, 575–590
56. Sabirov, R. Z., Merzlyak, P. G., Okada, T., Islam, M. R., Uramoto, H., Mori, T., Makino, Y., Matsuura, H., Xie, Y., and Okada, Y. (2017) The organic anion transporter SLCO2A1 constitutes the core component of the Maxi-Cl channel. *EMBO J.* **36**, 3309–3324
57. Sabirov, R. Z., Merzlyak, P. G., Islam, M. R., Okada, T., and Okada, Y. (2016) The properties, functions, and pathophysiology of maxi-anion channels. *Pflugers Arch.* **468**, 405–420
58. Saigusa, A., and Kokubun, S. (1988) Protein kinase c may regulate resting anion conductance in vascular smooth muscle cells. *Biochem. Biophys. Res. Commun.* **155**, 882–889
59. Toychiev, A. H., Sabirov, R. Z., Takahashi, N., Ando-Akatsuka, Y., Liu, H., Shintani, T., Noda, M., and Okada, Y. (2009) Activation of maxi-anion channel by protein tyrosine dephosphorylation. *Am. J. Physiol. Cell Physiol.* **297**, C990-1000
60. Nielsen, B. S., Hansen, D. B., Ransom, B. R., Nielsen, M. S., and MacAulay, N. (2017) Connexin Hemichannels in Astrocytes: An Assessment of Controversies Regarding Their Functional Characteristics. *Neurochem. Res.* **42**, 2537–2550
61. Connors, B. W. (2012) Tales of a Dirty Drug: Carbenoxolone, Gap Junctions, and Seizures. *Epilepsy Curr.* **12**, 66–68
62. Bai, D., del Corsso, C., Srinivas, M., and Spray, D. C. (2006) Block of specific gap junction channel subtypes by 2-aminoethoxydiphenyl borate (2-APB). *J. Pharmacol. Exp. Ther.* **319**, 1452–1458
63. Arensdorf, A. M., Marada, S., and Ogden, S. K. (2016) Smoothened Regulation: A Tale of Two Signals. *Trends Pharmacol. Sci.* **37**, 62–72

64. Ryan, K. E., and Chiang, C. (2012) Hedgehog secretion and signal transduction in vertebrates. *J. Biol. Chem.* **287**, 17905–17913
65. Fan, C. M., Porter, J. A., Chiang, C., Chang, D. T., Beachy, P. A., and Tessier-Lavigne, M. (1995) Long-range sclerotome induction by sonic hedgehog: direct role of the amino-terminal cleavage product and modulation by the cyclic AMP signaling pathway. *Cell*. **81**, 457–465
66. Hammerschmidt, M., Bitgood, M. J., and McMahon, A. P. (1996) Protein kinase A is a common negative regulator of Hedgehog signaling in the vertebrate embryo. *Genes Dev.* **10**, 647–658
67. Hynes, M., Porter, J. A., Chiang, C., Chang, D., Tessier-Lavigne, M., Beachy, P. A., and Rosenthal, A. (1995) Induction of midbrain dopaminergic neurons by Sonic hedgehog. *Neuron*. **15**, 35–44
68. Niewiadomski, P., Kong, J. H., Ahrends, R., Ma, Y., Humke, E. W., Khan, S., Teruel, M. N., Novitch, B. G., and Rohatgi, R. (2014) Gli protein activity is controlled by multisite phosphorylation in vertebrate Hedgehog signaling. *Cell Rep.* **6**, 168–181
69. Tuson, M., He, M., and Anderson, K. V. (2011) Protein kinase A acts at the basal body of the primary cilium to prevent Gli2 activation and ventralization of the mouse neural tube. *Dev. Camb. Engl.* **138**, 4921–4930
70. Vuolo, L., Herrera, A., Torroba, B., Menendez, A., and Pons, S. (2015) Ciliary adenylyl cyclases control the Hedgehog pathway. *J. Cell Sci.* **128**, 2928–2937
71. Cooper, D. M., Karpen, J. W., Fagan, K. A., and Mons, N. E. (1998) $Ca^{2+}$-sensitive adenylyl cyclases. *Adv. Second Messenger Phosphoprotein Res.* **32**, 23–51
72. DeCaen, P. G., Delling, M., Vien, T. N., and Clapham, D. E. (2013) Direct recording and molecular identification of the calcium channel of primary cilia. *Nature*. **504**, 315–318
73. Delling, M., DeCaen, P. G., Doerner, J. F., Febvay, S., and Clapham, D. E. (2013) Primary cilia are specialized calcium signalling organelles. *Nature*. **504**, 311–314
74. Moore, B. S., Stepanchick, A. N., Tewson, P. H., Hartle, C. M., Zhang, J., Quinn, A. M., Hughes, T. E., and Mirshahi, T. (2016) Cilia have high cAMP levels that are inhibited by Sonic Hedgehog-regulated calcium dynamics. *Proc. Natl. Acad. Sci. U. S. A.* **113**, 13069–13074
75. Lin, Y.-C., Niewiadomski, P., Lin, B., Nakamura, H., Phua, S. C., Jiao, J., Levchenko, A., Inoue, T., Rohatgi, R., and Inoue, T. (2013) Chemically inducible diffusion trap at cilia reveals molecular sieve-like barrier. *Nat. Chem. Biol.* **9**, 437–443
76. Burda, J. E., and Sofroniew, M. V. (2014) Reactive gliosis and the multicellular response to CNS damage and disease. *Neuron*. **81**, 229–248
77. Liddelow, S., and Barres, B. (2017) Reactive Astrocytes: Production, Function, and Therapeutic Potential. *Immunity*. 10.1016/j.immuni.2017.06.006
78. Davalos, D., Grutzendler, J., Yang, G., Kim, J. V., Zuo, Y., Jung, S., Littman, D. R., Dustin, M. L., and Gan, W.-B. (2005) ATP mediates rapid microglial response to local brain injury in vivo. *Nat. Neurosci.* **8**, 752–758
79. Shinozaki, Y., Shibata, K., Yoshida, K., Shigetomi, E., Gachet, C., Ikenaka, K., Tanaka, K. F., and Koizumi, S. (2017) Transformation of Astrocytes to a Neuroprotective Phenotype by Microglia via P2Y1 Receptor Downregulation. *Cell Rep.* **19**, 1151–1164

80. Elliott, M. R., Chekeni, F. B., Trampont, P. C., Lazarowski, E. R., Kadl, A., Walk, S. F., Park, D., Woodson, R. I., Ostankovich, M., Sharma, P., Lysiak, J. J., Harden, T. K., Leitinger, N., and Ravichandran, K. S. (2009) Nucleotides released by apoptotic cells act as a find-me signal to promote phagocytic clearance. *Nature*. **461**, 282–286
81. Koizumi, S., Shigemoto-Mogami, Y., Nasu-Tada, K., Shinozaki, Y., Ohsawa, K., Tsuda, M., Joshi, B. V., Jacobson, K. A., Kohsaka, S., and Inoue, K. (2007) UDP acting at P2Y6 receptors is a mediator of microglial phagocytosis. *Nature*. **446**, 1091–1095
82. Sims, J. R., Lee, S.-W., Topalkara, K., Qiu, J., Xu, J., Zhou, Z., and Moskowitz, M. A. (2009) Sonic hedgehog regulates ischemia/hypoxia-induced neural progenitor proliferation. *Stroke*. **40**, 3618–3626
83. Chen, S.-C., Huang, M., He, Q.-W., Zhang, Y., Opoku, E. N., Yang, H., Jin, H.-J., Xia, Y.-P., and Hu, B. (2017) Administration of sonic hedgehog protein induces angiogenesis and has therapeutic effects after stroke in rats. *Neuroscience*. **352**, 285–295
84. Malcuit, C., Kurokawa, M., and Fissore, R. A. (2006) Calcium oscillations and mammalian egg activation. *J. Cell. Physiol.* **206**, 565–573
85. Takayanagi, H., Kim, S., Koga, T., Nishina, H., Isshiki, M., Yoshida, H., Saiura, A., Isobe, M., Yokochi, T., Inoue, J., Wagner, E. F., Mak, T. W., Kodama, T., and Taniguchi, T. (2002) Induction and Activation of the Transcription Factor NFATc1 (NFAT2) Integrate RANKL Signaling in Terminal Differentiation of Osteoclasts. *Dev. Cell*. **3**, 889–901
86. Dolmetsch, R. E., Xu, K., and Lewis, R. S. (1998) Calcium oscillations increase the efficiency and specificity of gene expression. *Nature*. **392**, 933–936
87. Dolmetsch, R. E., Lewis, R. S., Goodnow, C. C., and Healy, J. I. (1997) Differential activation of transcription factors induced by $Ca^{2+}$ response amplitude and duration. *Nature*. **386**, 855–858
88. Colella, M., Grisan, F., Robert, V., Turner, J. D., Thomas, A. P., and Pozzan, T. (2008) $Ca^{2+}$ oscillation frequency decoding in cardiac cell hypertrophy: Role of calcineurin/NFAT as $Ca^{2+}$ signal integrators. *Proc. Natl. Acad. Sci.* **105**, 2859–2864
89. Hogan, P. G., Chen, L., Nardone, J., and Rao, A. (2003) Transcriptional regulation by calcium, calcineurin, and NFAT. *Genes Dev.* **17**, 2205–2232
90. Bannai, H., Hirose, M., Niwa, F., and Mikoshiba, K. (2019) Dissection of Local $Ca^{2+}$ Signals in Cultured Cells by Membrane-targeted $Ca^{2+}$ Indicators. *J. Vis. Exp. JoVE*. 10.3791/59246
91. Ito, J., Kato, T., Yamakawa, Y., Kato, H., Sakazaki, Y., Lim, R., and Tanaka, R. (1982) Interaction of glia maturation factor with the glial cell membrane. *Brain Res.* **243**, 309–314
92. Inoue, T. (2018) TI Workbench, an integrated software package for electrophysiology and imaging. *Microscopy*. **67**, 129–143
93. Samios, V. N., and Inoue, T. (2014) Interleukin-1β and interleukin-6 affect electrophysiological properties of thalamic relay cells. *Neurosci. Res.* **87**, 16–25
94. Hülsmann, S., Hagos, L., Heuer, H., and Schnell, C. (2017) Limitations of Sulforhodamine 101 for Brain Imaging. *Front. Cell. Neurosci.* 10.3389/fncel.2017.00044

95. Rasmussen, R., Nedergaard, M., and Petersen, N. C. (2016) Sulforhodamine 101, a widely used astrocyte marker, can induce cortical seizure-like activity at concentrations commonly used. *Sci. Rep.* **6**, 30433

**FOOTNOTES**

Abbreviations used are:

AC, adenylyl cyclase

2-APB, 2-aminoethyl diphenylborinate

ACSF, artificial cerebrospinal fluid

BBG, Brilliant Blue G

Ca, calcium

CBX, carbenoxolone

cAMP, cyclic AMP

CPN, cyclopamine

DMSO, dimethyl sulfoxide

ER, endoplasmic reticulum

GFAP, glial fibrillary acidic protein

HBS, HEPES-buffered saline

IP3R, inositol trisphosphate receptor

NFAT, nuclear factor of activated T cells

PBS, phosphate-buffered saline

PEI, poly-ethyleneimine

PKA, cAMP-dependent protein kinase

PTX, pertussis toxin

ROI, region of interest

RT, room temperature

SAG, Smoothened agonist

SHH, Sonic hedgehog

SMO, Smoothened

SR101, sulforhodamine 101

Tg, thapsigargin

TRP, transient receptor potential

TTX, tetrodotoxin

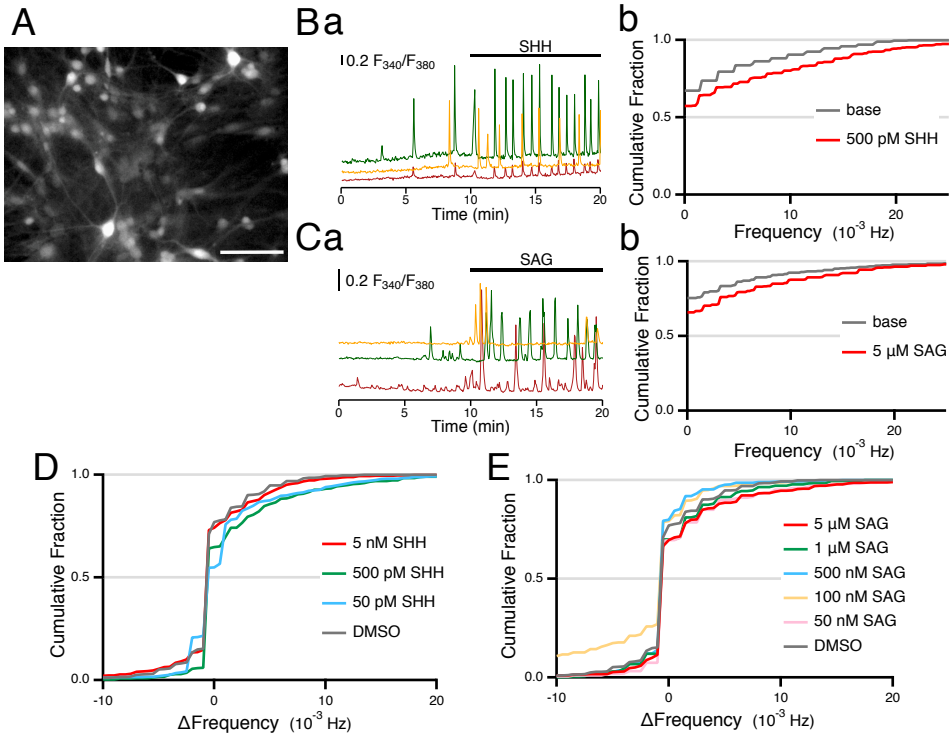


Figure 1. SHH and SAG increased Ca oscillation frequency in mouse hippocampal cultured cells.

(A) Hippocampal cells loaded with a Ca indicator, Fura-2. Scale bar, 100 μm. (B and C) Addition of SHH (Ba; 500 pM as final conc.) or SAG (Ca; 5 μM) evoked Ca oscillations. Frequency of Ca events in each cell was calculated before (base) and after the agonist applications. (Bb and Cb) Cumulative histograms during the baseline period and during agonist application periods are shown. Agonist-induced Ca frequency increase was evaluated by subtracting the baseline Ca frequency from that after the drug application in each cell (ΔFrequency). Cumulative histograms of ΔFrequency of cells applied with concentrations of SHH (D) or SAG (E) together with that of DMSO-applied control cells (0.1% as final conc., n = 820 cells from 7 cultures). Number of cells are: 5 nM SHH: n = 1688 cells from 16 cultures, 500 pM SHH: 510 cells from 5 cultures, 50 pM SHH: 603 cells from 5 cultures, 5 μM SAG: 1131 cells from 8 cultures, 1 μM SAG: 416 cells from 4 cultures, 500 nM SAG: 469 cells from 5 cultures, 100 nM SAG: 560 cells from 6 cultures, and 50 nM SAG: 428 cells from 4 cultures.

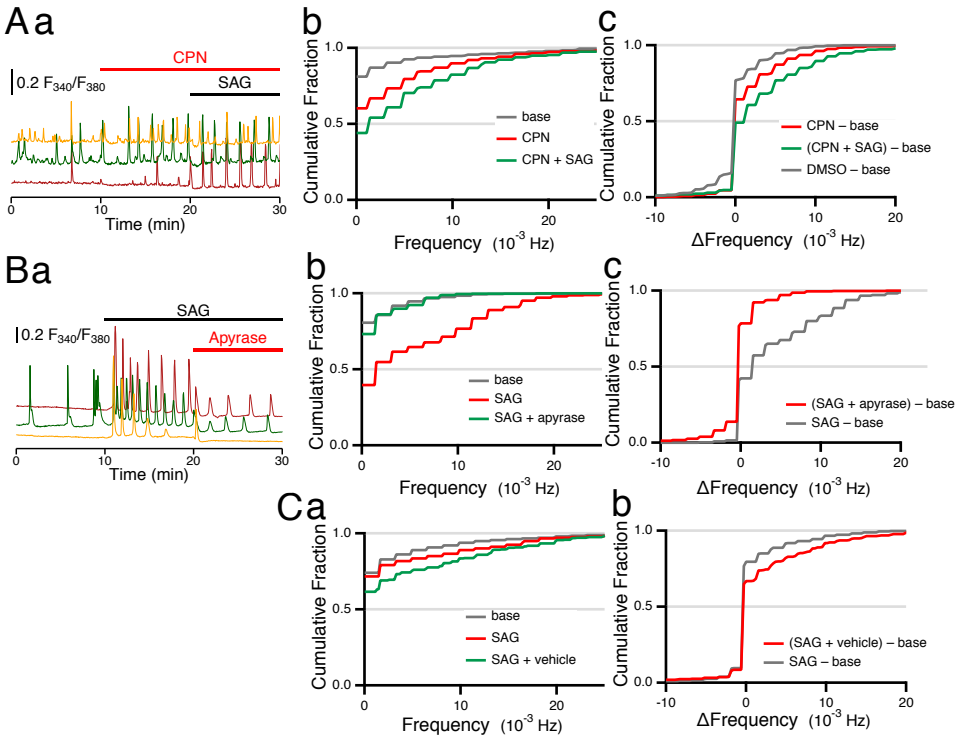


Figure 2. Effects of cyclopamine and apyrase against the SAG-induced enhancement of Ca oscillation frequency in hippocampal primary culture.

(Aa) Cyclopamine (CPN; 5 μM) was added to the bath, and SAG application followed. (Ab) Cumulative histograms of the Ca oscillation frequency during the baseline period (base), CPN and CPN with SAG (n = 768 cells from 6 cultures). (Ac) ΔFrequency of the drug effects are displayed as cumulative histograms, together with that of a control cell group to which 0.1% DMSO was added in place of CPN, which is the same one shown in Fig. 1D and E. (Ba) Apyrase (5 U/mL) suppressed the SAG-induced enhancement of Ca oscillation frequency. (Bb) Cumulative histograms of Ca oscillation frequency during the baseline period, after SAG application and after apyrase addition (n = 444 cells from 3 cultures). (Bc) Cumulative histograms of ΔFrequency. (C) As a control, vehicle solution (HBS-TTX) was added in place of apyrase in (B). Cumulative histograms of Ca event frequency (Ca) and ΔFrequency (Cb) are shown (n = 729 cells from 7 cultures).

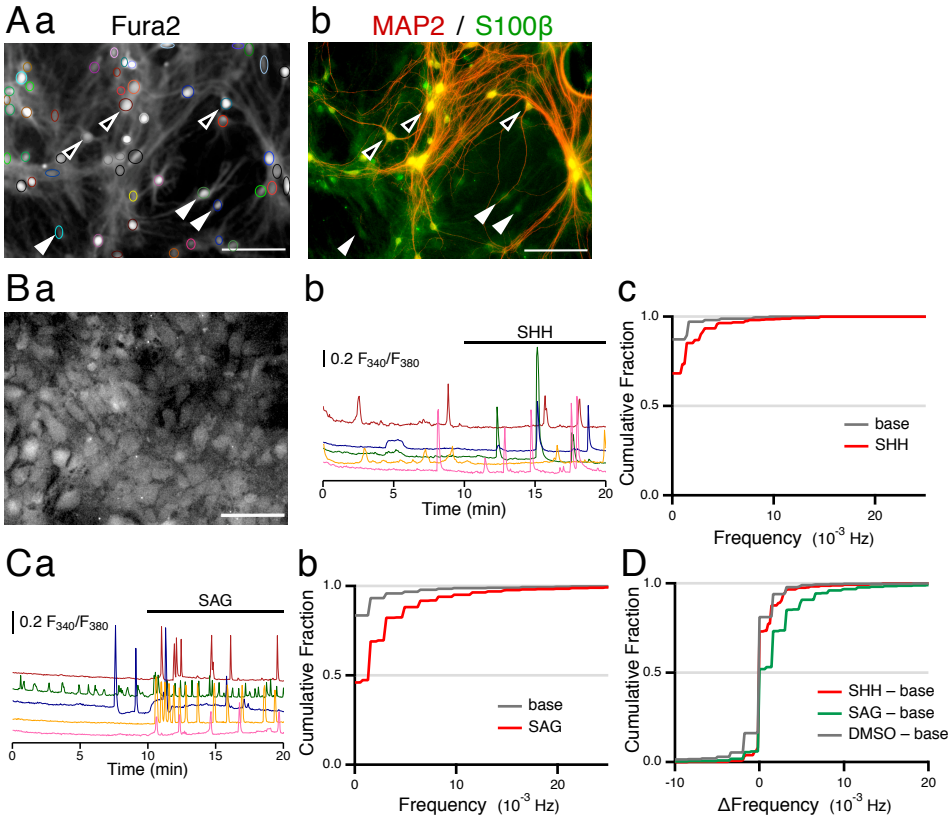


Figure 3. The SAG-induced Ca oscillation enhancement takes place in astrocytes

(A) Cell types showing Ca oscillations were characterized by immunohistochemistry. Time lapse Ca imaging of a 10 min baseline (HBS-TTX) and 10 min in SAG was performed in hippocampal cultures (Aa), which were then fixed and stained with anti-MAP2 (red) and anti-S100β (green) antibodies (Ab). Filled arrowheads indicate S100β-positive cells, and open arrowheads indicate MAP2-positive cells. Scale bar, 100 µm. (Ba) Fura-2-loaded astrocyte culture. The enhancing effects of SHH (B; 500 pM, n = 465 cells from 5 cultures) or SAG (C; 5 µM, n = 1731 cells from 12 cultures) on Ca oscillation frequency were observed in the astrocyte culture. (D) Cumulative histograms of ΔFrequency of SHH and SAG together with a DMSO (0.1%) applied control cell group (n = 642 cells from 5 cultures).

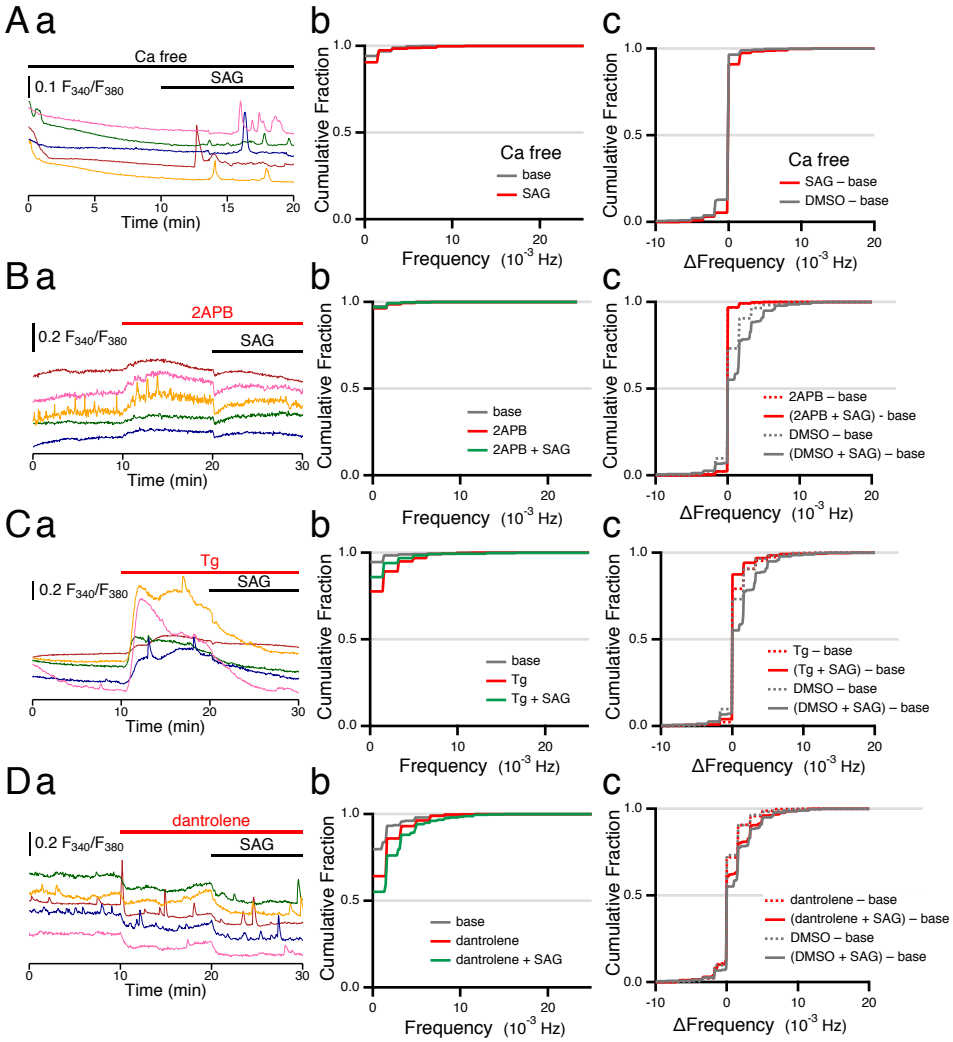


Figure 4. Ca release through IP3R is involved in the SAG-enhanced Ca oscillations

(Aa) The SAG-induced Ca oscillation frequency enhancement was tested in Ca-free media, in which Ca-free HBS supplemented with EGTA (1 μM) was used as an extracellular medium throughout the recording period. (Ab) Cumulative histograms of Ca oscillation frequency with Ca-free medium during the baseline period and after the application of SAG (n = 431 cells from 5 cultures). (Ac) A cumulative histogram of ΔFrequency(SAG – base) in Ca-free medium and ΔFrequency(DMSO – base) obtained from a control group with DMSO (0.1% in Ca-free medium) in place of SAG (n = 377 cells from 4 cultures). (B-D) 2-APB (B; 50 μM, n = 417 cells from 5 cultures), an IP3R inhibitor, Thapsigargin (Tg; C; 100 nM, n = 416 cells from 5 cultures), an inhibitor to the endoplasmic reticulum Ca-ATPase, or Dantrolene (D; 10 μM, n = 505 cells from 5 cultures), a ryanodine receptor antagonist, was applied and addition of SAG followed. (Bb, Cb, Db) Cumulative histograms of Ca oscillation frequency during the baseline period, after antagonist application and after SAG addition. (Bc, Cc, and Dc) Cumulative histograms of ΔFrequency together with those obtained from a control cell group with DMSO in place of the antagonists (n = 384 cells from 4 cultures).

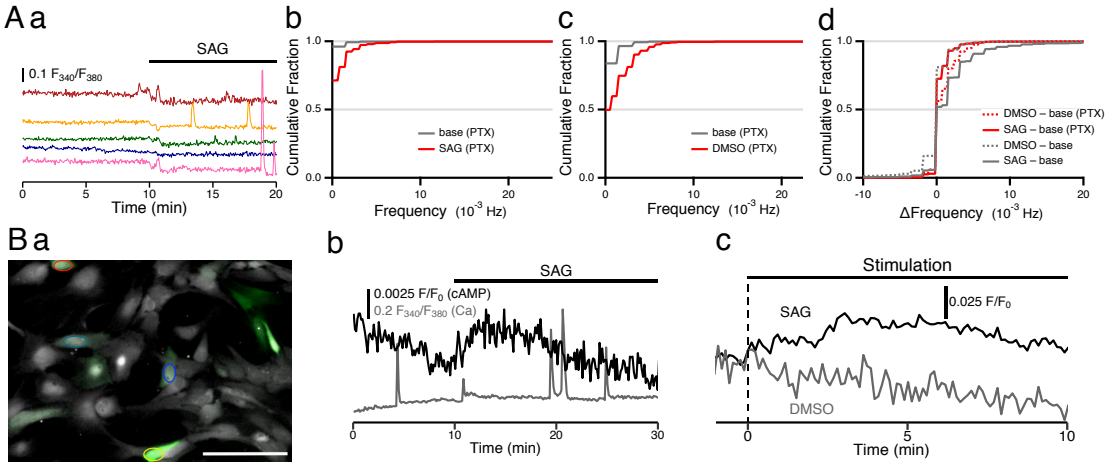


Figure 5. The SAG-induced enhancement of Ca oscillations requires Gi activation

(A) Astrocyte cultures were treated with 100 ng/ml pertussis toxin (PTX) for 24 h prior to Ca imaging. (Aa) SAG increased the Ca oscillation frequency compared to baseline. (Ab-c) Cumulative histograms of Ca oscillation frequency during the baseline period and after SAG (Ab, n = 714 cells from 7 cultures) or control DMSO (Ac, n = 537 cells from 4 cultures) application. (Ad) Cumulative histograms of ΔFrequency together with those from the control cell group shown in Fig. 3D. (B) cAMP imaging revealed an increase in intracellular cAMP concentration ($[cAMP]_i$). (Ba) A cAMP indicator, Flamindo-2 (green), was expressed in astrocytes and Fura-2 (gray) was loaded for simultaneous measurement. Scale bar, 100 µm. (Bb) Time course of $[cAMP]_i$ and $[Ca]_i$ were monitored before and after SAG application. (Bc) Averaged time course of Flamindo-2 signal from astrocytes to which SAG (n = 97 cells from 8 experiments) or vehicle (0.1% DMSO; n = 58 cells from 4 experiments) was applied.

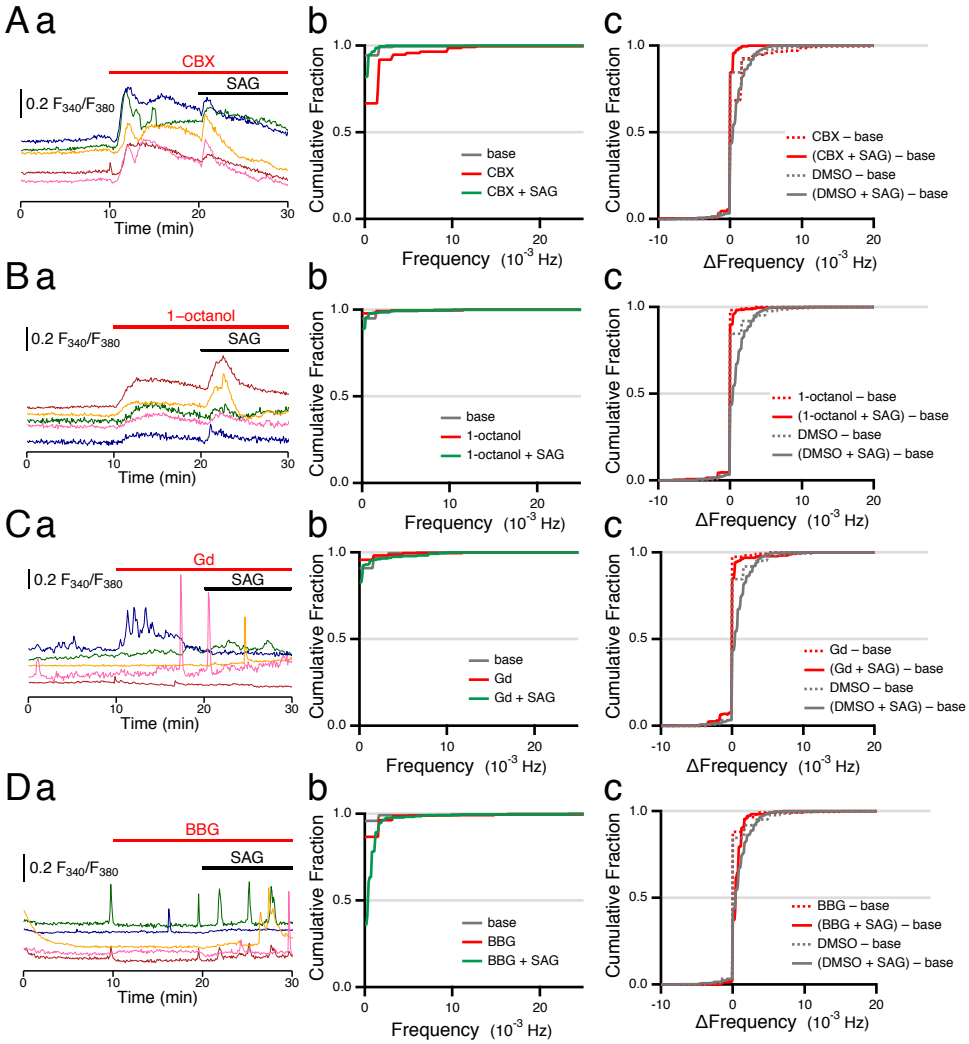


Figure 6. Blockers of ATP release channels altered the SAG-induced Ca oscillation frequency enhancement

(a) Carbenoxolone (A; CBX, 100 μM, n = 231 cells from 4 cultures), a connexin hemichannel inhibitor, 1-octanol (B; 2 mM, n = 274 cells from 5 cultures), an inhibitor to the connexin hemichannel, $Gd^{3+}$ (C; 50 μM, n = 229 cells from 4 cultures), an inhibitor to the Maxi-anion channel, or brilliant blue G (D; BBG, 1 μM, n = 292 cells from 5 cultures), a P2X7 receptor antagonist, was applied and addition of SAG followed. (b) Cumulative histograms of Ca oscillation frequency before application of the blockers, under the blockers, and after SAG addition. (c) Cumulative histograms of ΔFrequency together with those from a control cell group in which 0.1% DMSO was applied in place of the blockers (n = 368 cells from 5 cultures).

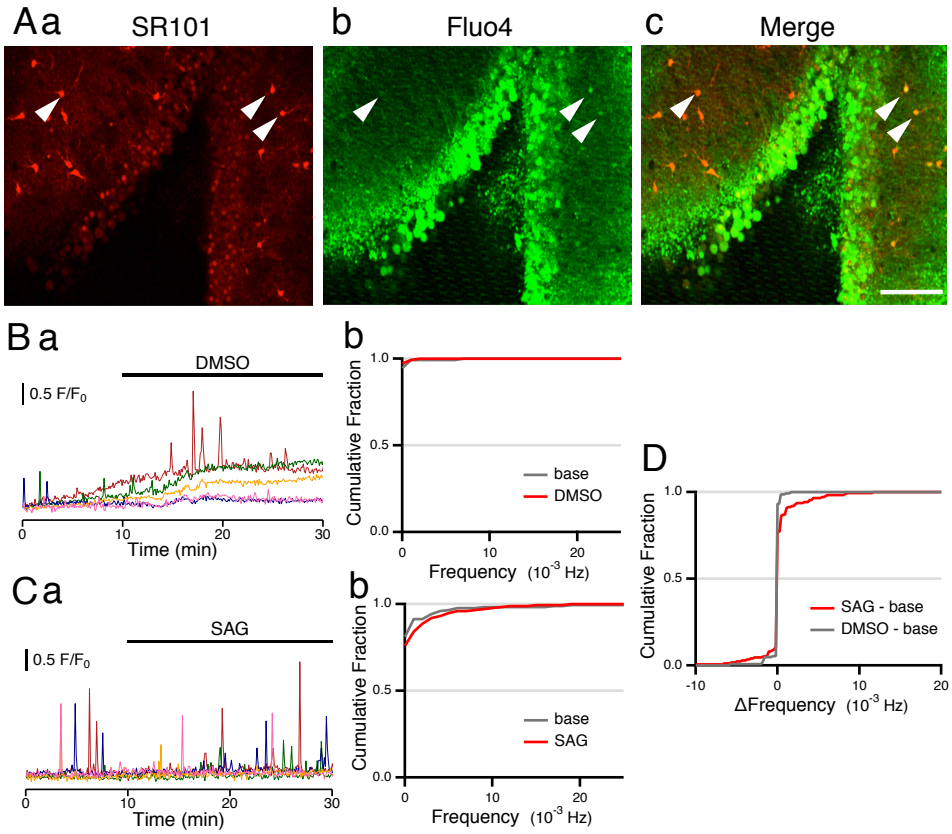


Figure 7. Enhancement of Ca oscillation in astrocytes in brain slices

(A) Astrocytes in an acute hippocampal slice were stained with an astrocyte marker, SR101 (red), and a Ca indicator, Fluo-4 (green). Arrow heads point SR101 and Fluo-4 double-positive cells. Scale bar, 100 µm. Ca oscillations by the application of 0.1% DMSO (B; n = 167 cells from 8 slices) and 50 nM SAG (C; n = 175 cells from 9 slices). (D) Cumulative histograms of ΔFrequency.

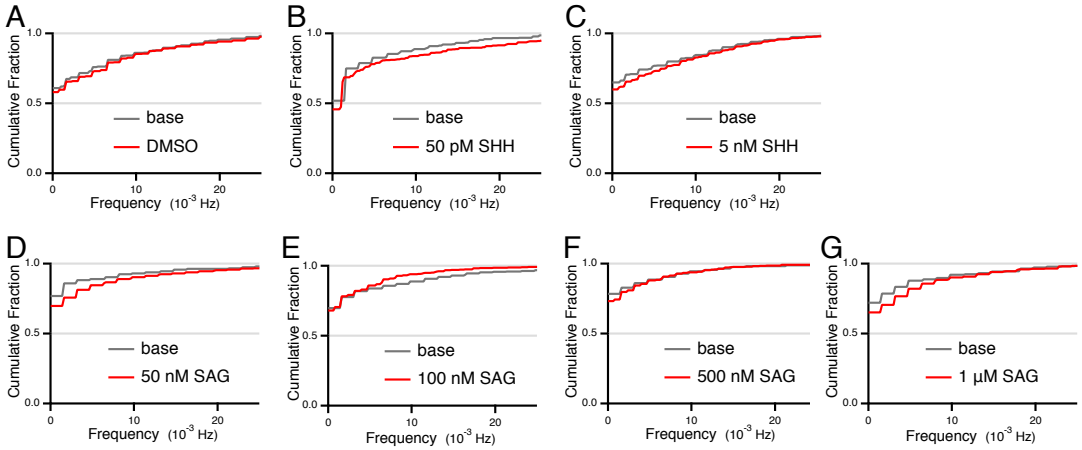


Figure S1. Dose-response relationships between the SHH and SAG concentrations and Ca oscillation frequency in hippocampal culture cells

Calcium oscillation frequencies in hippocampal culture cells were measured before and after the application of SHH, SAG, and DMSO (0.1%) for control. Cumulative histograms of each condition indicate effects of DMSO (A; $p = 0.11$, $n = 820$ cells from 7 cultures), 50 pM SHH (B; $p = 0.38$, $n = 603$ cells from 5 cultures), 5 nM SHH (C; $p < 0.01$, $n = 1688$ cells from 16 cultures), 50 nM SAG (D; $p < 0.05$, $n = 428$ cells from 4 cultures), 100 nM SAG (E; $p = 0.85$, $n = 560$ cells from 6 cultures), 500 nM SAG (F; $p = 0.13$, $n = 469$ cells from 5 cultures), and 1 µM SAG (G; $p < 0.05$, $n = 416$ cells from 4 cultures). Results with 500 pM SHH and 5 M SAG are indicated in Fig. 1Bb and 1Cb, respectively.

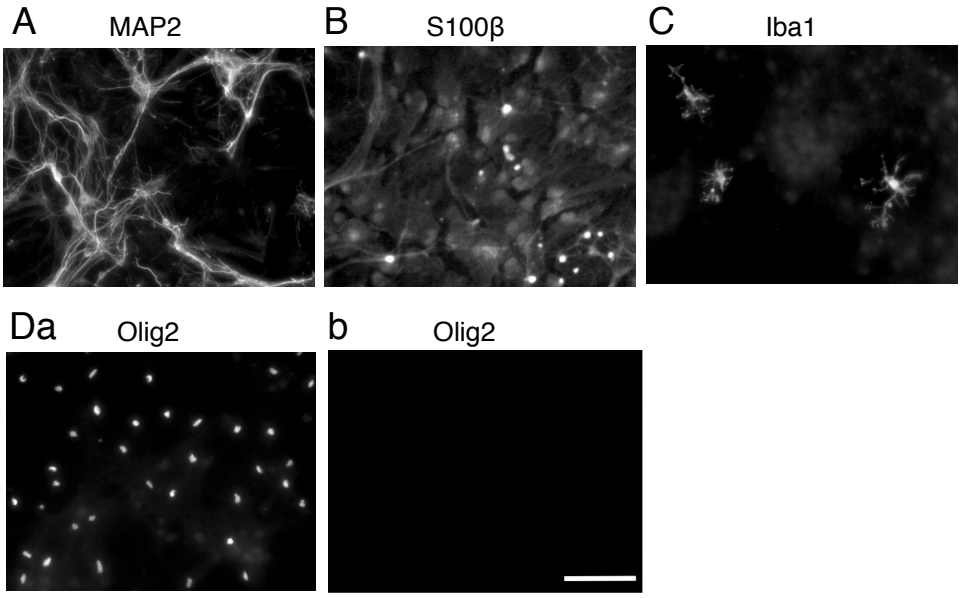


Figure S2. Identification of cell types in the mouse hippocampal culture

Immunohistochemistry was performed on mouse hippocampal cultures with antibodies against MAP2 (A; neuronal marker), S100β (B; astrocyte marker), Iba1 (C; microglia marker) and Olig2 (D; oligodendrocyte marker). MAP2- and S100β-positive cells were observed everywhere over coverslips. Iba1-positive cells were found only in culture batch (10-20 cells in total in each coverslip) out of 3 batches. Olig2-positive cells were found only where neuron density was very high (Da), but not at all in view fields where neuron density was modest (Db). Scale bar, 100 µm.

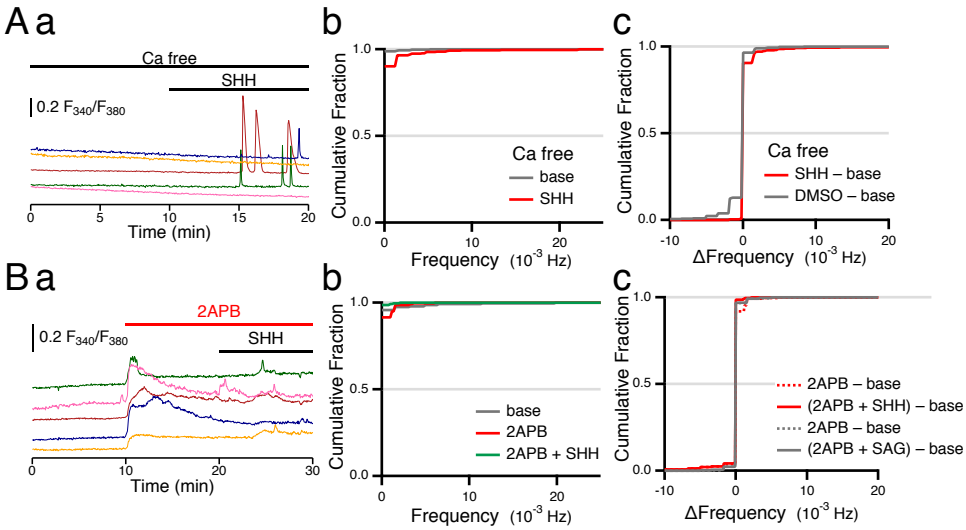


Figure S3. The SHH induced Ca oscillation frequency enhancement was not affected by extracellular free Ca but by 2-APB in astrocytes

(Aa) The SHH-induced enhancement of Ca oscillation frequency in astrocytes was not affected by the removal of extracellular Ca, in which Ca-free HBS supplemented with 10 μM EGTA was used as an extracellular medium throughout the recording period. (Ab) Cumulative histograms of Ca oscillation frequency with Ca-free medium during the baseline period and after SHH application show a right-shift of the histogram by SHH ($p < 0.001$, $n = 431$ cells from 5 cultures), (Ac) Cumulative histograms of ΔFrequency calculated from the cell group in (Ab) and from a control cell group shown in Fig. 4Ac show an apparent difference ($p < 0.001$). (Ba) 2-APB (50 μM), an IP3R inhibitor, blocked the SHH-induced Ca oscillation enhancement. (Bb) Cumulative histograms of Ca oscillation frequency during the baseline period, after 2-APB application and after SHH application show SHH did not take effect in 2-APB (base vs. 2-APB: $p = 0.08$, base vs. SHH: $p = 0.046$, 2-APB vs. SHH: $p < 0.001$, $n = 237$ cells from 4 cultures). (Bc) Cumulative histograms of ΔFrequency(2-APB – base) and ΔFrequency[(2-APB + SHH) – base] are shown together with ΔFrequency histograms from a cell group applied SAG in place of SHH shown in Fig. 4Bc.

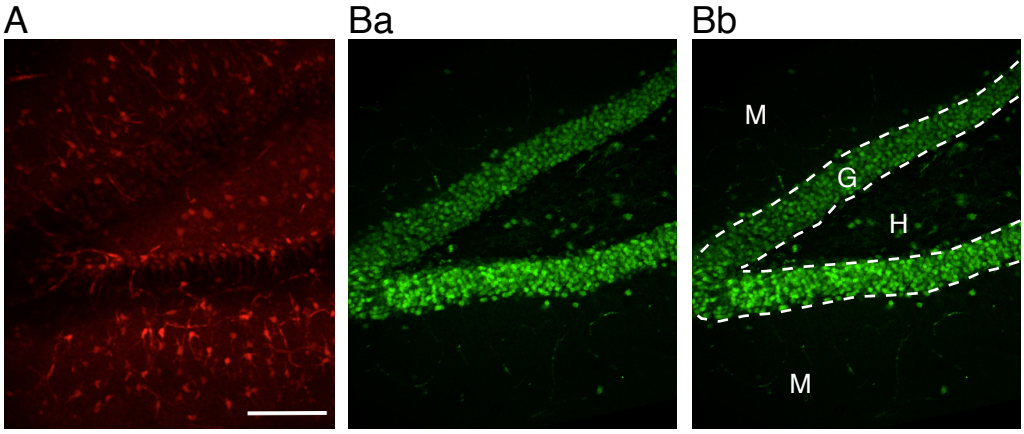


Figure S4. SR101-staining and immunostaining with anti-NeuN antibody of a hippocampal slice

(A) A 20 µm-thick z-stack image taken from a live hippocampal slice stained with SR101. Scale bar: 100 µm. (Ba) A 20 µm-thick z-stack image taken from the same slice after fixation and immunohistochemistry with anti-NeuN-antibody. (Bb) M: molecular layer, G: granule cell layer, and H: hiles.

Methods: Hippocampal slices were prepared and stained with SR101 as described in Experimental Procedures. After obtaining the SR101 image under the 2-photon microscope, slices were fixed in 4% paraformaldehyde for overnight at 4°C, followed by blocking with 10% blocking solution (10% BSA and 0.3% Triton X-100 in PBS) for 1 h at RT. Then slices were incubated with anti-NeuN antibody (1:500; MAB377; Millipore, Tokyo, Japan) overnight at RT then with a secondary antibody (Donkey anti-mouse IgG conjugated with Alexa Fluor 488; ac150101; abcam) for overnight at RT. Both SR101-stained and immunostained images were constructed by maximum intensity z-projections of 10 two-photon images with 2 µm z-interval.

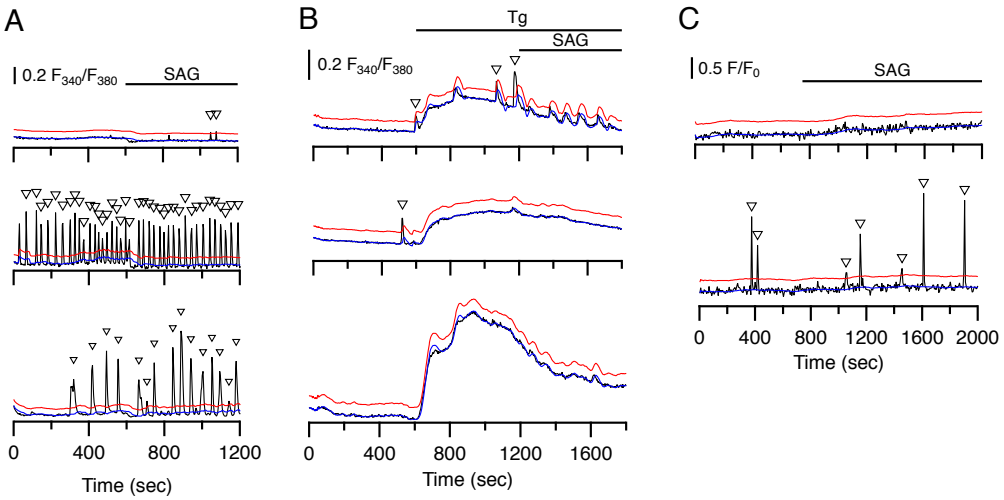


Figure S5. Ca event detection methods

Baseline values for each data point in each ROI were determined (blue), which well traced the resting Ca signal changes, and threshold by adding a fixed value to the baseline values (red) was used to detect Ca events. (A) In most of the cell culture experiments, baseline values were calculated by averaging preceding data points (see Experimental Procedures), which overlapped well with the baseline even with high frequency Ca oscillations (middle trace). Threshold was set by adding a fixed value (0.08) to the calculated baseline values and Ca events were faithfully picked up (triangle marks). (B) In experiments using 2-APB, Tg, CBX and 1-octanol, where the Fura-2 ratio drifted because of the reagents, baseline values were calculated using not average but linear regression of preceding data points to cancel the slow signal drift. Here Ca time courses of cells applied with Tg are shown. (C) In the slice experiments, baseline was calculated as above with the $F/F_0$ Fluo-4 fluorescence. Threshold was set by adding 0.3 to the calculated baseline.